Università degli Studi di Padova

DIPARTIMENTO DI FISICA E ASTRONOMIA

Corso di Laurea in Fisica

Data analysis of an optical emission spectroscopy diagnostic in NIO1 experiment

Laureando:

Luca Vialetto

Matricola 1049018

Relatore:

Dott. Gianluigi Serianni

Correlatore:

Dott.ssa Barbara Zaniol

Anno Accademico 2014–2015

Abstract

Neutral Beam Injectors (NBI's) will play a key role in future fusion reactors, but many open issues are still to be solved. Consorzio RFX in Padova will host the test bed for ITER NBI's, with the aim of demonstrating the reliability of the present NBI design and of optimizing the performances. For this reason, another more flexible experiment has started named NIO1 (Negative Ion Optimization phase 1). In the process to study these new concepts and solutions, the measurements of the plasma parameters and of the extracted beam are of fundamental importance. A key diagnostic is the Optical Emission Spectroscopy (OES): its exploitation on NIO1 is the subject of this thesis. An overview of OES measurements and the methods adopted to analyze them will be given in the following chapters. Some of the plasma parameters could be deduced from OES only by comparison with the predictions of radiative models. The collisional radiative model that has been applied in this thesis is called YACORA and has been developed by IPP Garching. Here is an outline of the thesis:

Chapter 1: Introduction to the physics of controlled thermonuclear fusion and the structure of neutral beam injectors.

Chapter 2: A general overview of NIO1 experiment, diagnostic methods, in particular the Optical Emission Spectroscopy. Also the CR model is presented.

Chapter 3: Analysis of measurements in air as a working gas. Both high and low resolution spectrometers are utilized. The main results are presented, such as electron temperature (T_e), vibrational temperature (T_v) and rotational temperature (T_r).

Chapter 4: The analysis of measurements with hydrogen as a working gas is presented. The main quantities obtained with measurements of low resolution spectrometer are: electron density (n_e) and electron temperature (T_e) along the LOS (line of sight) and Dissociation degree (n_H/n_{H_2}). These are obtained by the method of *line ratio* and with the use of the CR model. The results and the errors of these estimates are presented and discussed.

Sommario

Gli Iniettori di Neutri avranno un ruolo fondamentale nei futuri reattori a fusione, ma molte sono le questioni aperte che necessitano una soluzione. Il Consorzio RFX a Padova ospiterà il banco di prova degli iniettori di ITER, il cui scopo è dimostrare l'affidabilità del modello dei presenti iniettori di neutri e ottimizzarne le performaces. Per questo motivo, è entrato in funzione un esperimento più flessibile di nome NIO1 (Negative Ion Optimization fase 1). Nel contesto dello studio di nuovi concetti e soluzioni, le misure dei parametri di plasma e del fascio estratto sono di fondamentale importanza. Una delle diagnostiche chiave è la Spettroscopia di Emissione Ottica (OES): il suo utilizzo nel contesto dell'esperimento NIO1 è lo scopo di questa tesi. Nei seguenti capitoli sarà fornita una panoramica delle misure di OES e dei metodi di analisi dati. Alcuni parametri di plasma possono essere dedotti solo tramite il confronto con le previsioni di un modello. Il modello Collisionale-Radiativo che è stato applicato in questa tesi è chiamato YACORA ed è stato sviluppato ad IPP Garching. La descrizione della struttura della tesi è la seguente:

Capitolo 1: Introduzione sulla fisica della fusione termonucleare controllata e sulla struttura degli iniettori di neutri.

Capitolo 2: E' presentata una panoramica sull'esperimento NIO1, sulle diagnostiche applicate, in particolare sulla spettroscopia di emissione ottica. Il modello Collisionale-Radiativo è presentato alla fine del capitolo.

Capitolo 3: Analisi delle misure raccolte utilizzando l'aria come gas di riempimento. Nella raccolta dati sono stati utilizzati spettrometri sia ad alta che a bassa risoluzione. Sono presentati i risultati principali, come la temperatura elettronica (T_e), la temperatura vibrazionale (T_v) e la temperatura rotazionale (T_r).

Capitolo 4: Analisi delle misure raccolte utilizzando idrogeno come gas di riempimento. Le principali quantità ottenute con spettrometri a bassa risoluzione sono: densità elettronica (n_e) e temperatura elettronica (T_e) lungo la linea di vista (LOS) a il grado di dissociazione (n_H/n_{H_2}). Questi risultati sono ottenuti tramite il metodo del *rapporto di riga* e tramite l'utilizzo del modello Collisionale-Radiativo. Sono presentati e discussi i risultati ottenuti e le rispettive stime degli errori.

Contents

Chapter 1

Introduction

1.1 Fusion Energy

It is well known that a large part of the world is in a difficult energy situation. Virtually all projections of future energy consumption conclude that global energy demand has tripled in the past 50 years and might double in the next 30 years [1]. Population growth and increases in income per person are the key drivers behind the rising demand for energy.

A crucial point related to the energy supply concerns the environment. In particular global greenhouse-gas emissions and air pollution continue to increase in many of the world's fast-growing cities. Figure 1.1 shows the principal sources of energy used in the world: about 80% of our energy comes from *fossil fuels* (such as coal, natural gas or oil). The problem is that burning any fossil fuel leads to the generation of carbon dioxide (CO_2) which is largely responsible for the greenhouse effect. There is no obvious single solution, but one of the alternatives to burning fossil fuels is *nuclear fusion*. The fusion mechanism is based on the merging of light elements, mainly hydrogen (H)

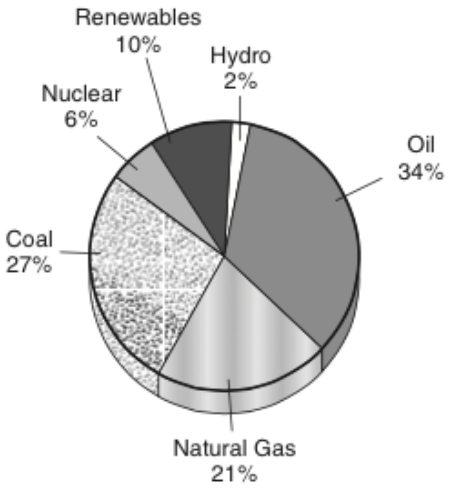

Figure 1.1: Energy consumption by source for the world, from [1]

and its isotopes: deuterium (D) and tritium (T). A fusion reaction is possible if two light nuclei fuse into a nucleus below an atomic mass of A=56. Because of the increase in binding energy, the final state is more stable and the difference of mass (Δm) between the initial and final states is transformed into energy (E) according to the Einstein's relation: $E = \Delta m \cdot c^2$.
A fusion reaction can typically be written as:

$$ {}^{a}_{z}X + {}^{A-a}_{Z-z}Y \longrightarrow {}^{A}_{Z}Z + Q $$

where $Q > 0$ is the energy released and it is given by: $Q = [(m_X + m_Y) - m_Z] \cdot c^2$. Since nuclear interaction is a short range interaction, this process can be obtained only if the two nuclei involved have enough kinetic energy to overcome the Coulomb barrier. Studies of nuclear properties of light elements indicate that three reactions may be more advantageous for the production of energy [2].

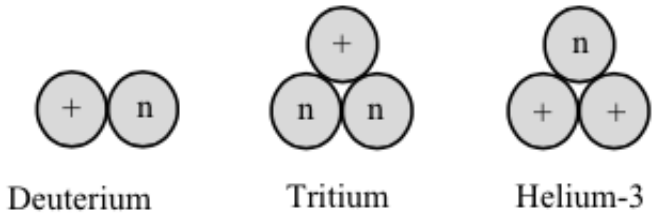

Figure 1.2: Nuclear structure of the basic fusion fuels

The D-D reaction: It has two channels, each occurring with approximately equal probability:

$$ D + D \longrightarrow He^3 + n + 3.27MeV $$

$$ D + D \longrightarrow T + p + 4.03MeV $$

These two reactions are the most difficult to initiate, but the main advantages is that D occurs naturally in ocean water. In fact, there is one atom of deuterium per 6700 atoms of hydrogen.

The D-He^3 reaction: The energy produced per reaction is impressive but there are no natural supplies of He^3 on Earth.

$$ D + He^3 \longrightarrow \alpha + p + 18.3MeV $$

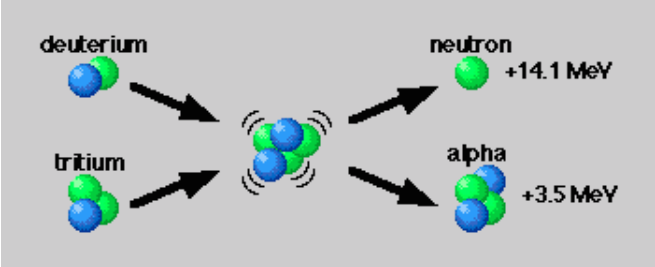

Figure 1.3: The deuterium-tritium reaction

The D-T reaction:

$$D + T \longrightarrow \alpha + n + 17.6MeV$$

The main advantage is that this reaction occurs at faster rate, but there is no natural tritium on Heart. Furthermore, the tritium is radioactive with a half life of 12.26 years. The solution is to use a chemical element might breed tritium such as lithium. The nuclear reactions involved are:

$$_3Li^6 + n(slow) \longrightarrow \alpha + T + 4.8MeV,$$

$$_3Li^7 + n(fast) \longrightarrow T + \alpha + n - 2.5MeV$$

The first reaction generates energy while the second consumes energy. Nuclear data show that the $_3Li^6$ reaction is much easier to initiate. Because of the large energy release (and since the Coulomb barrier is not higher than in the D-D reactions), the D-T reaction has been selected for use in controlled fusion reactors.

1.2 What is a plasma?

A plasma is a quasi-neutral gas of charged and neutral particles which exhibits collective behavior [3].

Explicit criteria that allow to quantify when this definition is valid are based on two basic parameters: a characteristic scale length (the *Debye length* λ_D), a characteristic inverse time scale (the *plasma frequency* ω_p) [2]. The main criteria used to define a plasma are:

1. Plasma behavior requires small Debye length $\lambda_D << L$ where L is the typical dimensions of the ionized gas and high plasma frequency $\omega_p >> \omega_T$ where ω_T is the inverse time for a particle to move across

the plasma. If this requirements is fulfilled, the plasma is effectively shielded out from electric fields over a distance equal to the Debye length. If the shielding of electric field is extremely efficient, the local number densities of electrons and ions are barely perturbed. Thus, the *local* electron density is almost equal to the *local* ion density over almost the entire plasma volume: $n_e(x) \sim n_i(x)$. This local property is known as *quasi-neutrality*

2. For a statistical fluid description of plasma behavior, large values of Λ_D is required. This parameter represents the number of charged particles in a sphere whose radius is equal to the Debye length. The fluid model implies that the plasma is described by a large number of fluid volumes elements that have to be small enough in order to provide a good spatial resolution, on the other hand the volumes must contain large number of particles for averaging the charge and current densities into a smooth function

3. In a plasma low collisionality is required since long-range collective effects dominate plasma behavior instead of short-range interactions, such as microscopic Coulomb collisions. In order to quantify this condition, the plasma frequency ω_p must be larger than the collision frequency ν_c

Plasma densities and temperatures cover several order of magnitudes, the following table lists the principal parameters for various types of plasmas [3]:

Type	Density(m^{-3})	k_BT(eV)
Typical fusion reactor	10^{21}	10000
Typical ionosphere	10^{11}	0.05
Typical glow discharge	10^{15}	2
Typical flame	10^{14}	0.2
Interplanetary space	10^{6}	0.01

1.3 The Challenge of ITER

On 25 April 2007, the IAEA, International Atomic Energy Agency, promulgated a document called "Agreement on the Establishment of the ITER International Fusion Energy Organization for the Joint Implementation of ITER Project" in which the ITER Project is defined as [7]:

> *An international project that aims to demonstrate the scientific and technological feasibility of fusion energy for peaceful purposes.*

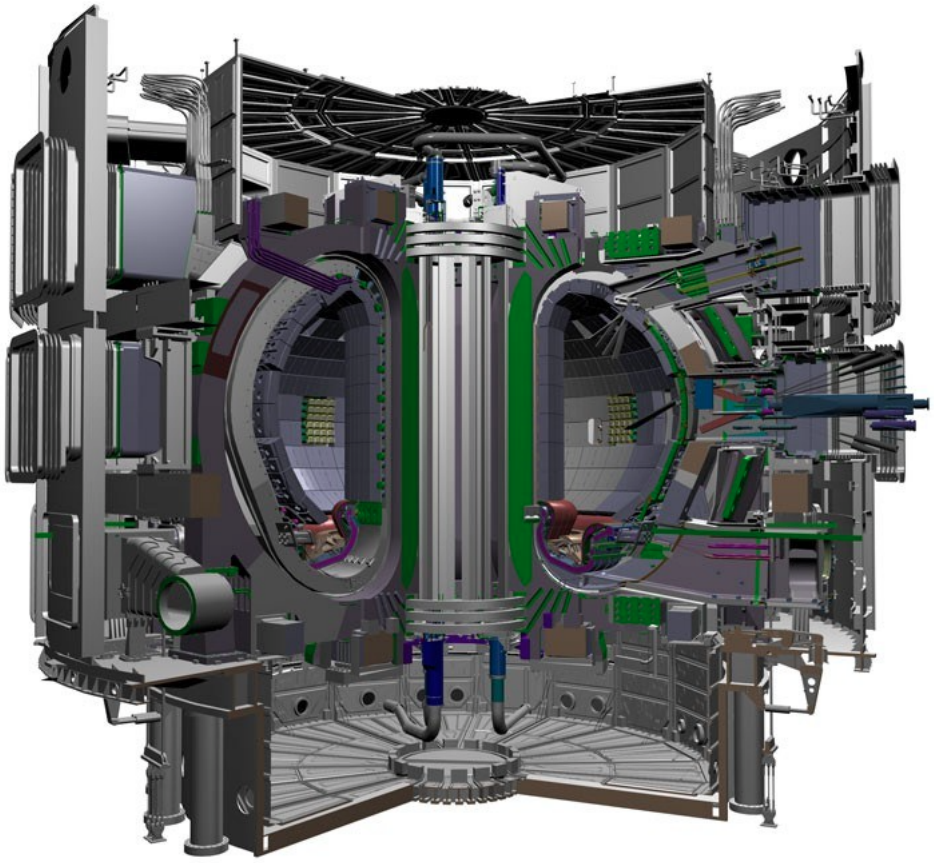

Figure 1.4: The ITER device, from [4]

ITER is a machine where the plasma is confined by a toroidally shaped magnetic field. The aim of ITER, which is under construction in Southern France (Cadarache), is to produce half a GW of fusion power (with 10 times more energy produced by fusion than the energy injected into the plasma to maintain the fusion reactions) from a burning plasma. The following table reports the main parameters of ITER:

Basic Parameters:	
Plasma Mayor Radius	6.2 m
Plasma Current	15.0 MA
Toroidal Field on Axis	5.3 T
Fusion Power	500 MW
Power Amplification	$Q > 10$

It is interesting to see what ITER may actually achieve in a simulation of 2009 by a group of Princeton (Fig. 1.5).

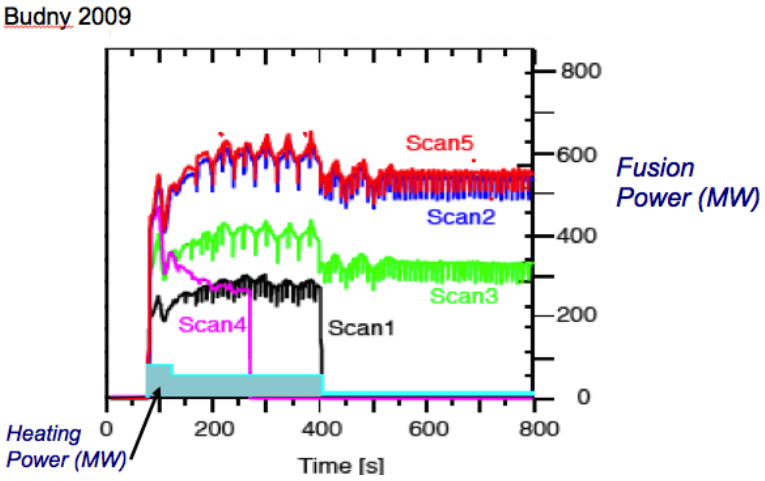

Figure 1.5: The ITER modeling, R.V. Budny, Princeton Plasma Physics Laboratory, 2009 [5] [6]

Figure 1.5 reports the fusion power that can be produced in different ITER scenarios (scan 1-5). All scenarios foresee at the beginning an input heating power (light blue in the picture) that helps increasing the plasma temperature and makes the fusion reactions start. The success of the fusion reaction depends on the capability to trap the alpha particles energy inside the plasma (scan 2-5 versus scan 1). In fact, a D-T reaction produces an α-particle with 3.5 MeV that slows down into the plasma and gives up this energy. This capability is also necessary to reach an auto sustained steady state condition when the external heating is turned off at 400 s. In scan 3 a 20% of reduction of the edge temperature has been simulated, while in scan 4 it can be seen what happens if the fusion reaction turns off due to the 'ash' of α-particles. In this simulation, the importance of external heating is highlighted. ITER will have three sources of auxiliary power: 33 MW of negative-ion-driven neutral beams, 20 MW of ICH (ion-cyclotron heating) and 20 MW of ECH (electron cyclotron heating).

1.4 Heating and Current Drive Systems

One of the most important topics involving fusion reactors is to heat plasma particles because the thermal energy is used to overcome the Coulomb barrier that inhibits fusion. Another important topic is current drive. In fact, magnetic fusion reactors require some non-inductive means to drive a toroidal

current which is necessary to develop a steady state device. Some methods of heating and current drive that are being developed in laboratory experiments are [2]:

Ohmic heating: The current that flows in most magnetic configurations ohmically heats the plasma; unfortunately at higher temperature this method becomes less effective because the resistivity of the plasma decreases with temperature.

RF waves: High-frequency electromagnetic waves are injected into the plasma. There is a strong absorption of energy which is converted into heat. RF waves drive the electrons and induce a toroidal current.

Neutral Beam Injectors: A beam of ions is accelerated by electrostatic fields and then neutralized, since the reactor magnetic field would deflect the beam well before entering the plasma. The neutral atoms lose energy to the plasma through Coulomb scattering from ions and electrons. The neutral beam is injected tangentially into the plasma, generating a toroidal momentum parallel to the direction of injection that is transferred partially to electrons though collisions. These electrons constitute an electric current flowing in the toroidal direction. Because of the aim of this thesis I will focus on this method that is presented in the following subsections

1.4.1 Structure of a NBI (Neutral Beam Injector)

In the structure of a NBI four elements can be identified [8]:

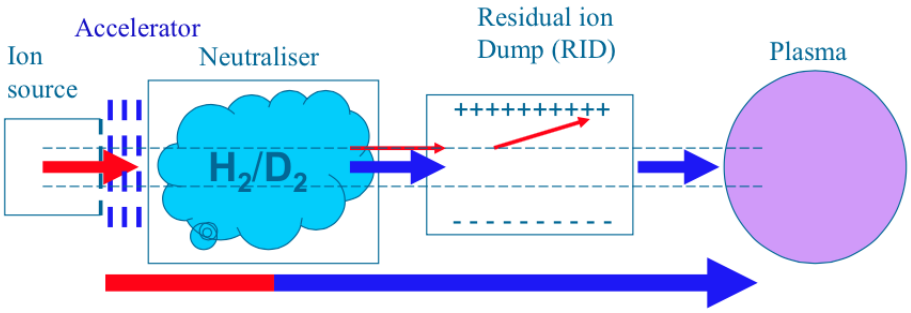

Figure 1.6: The structure of a NBI

1. Ion Source: It is often a plasma-based source which means that it uses a plasma to ionize the species (H_2 or D_2) and to produce low-temperature ions. Either positive or negative ions can be produced in

low temperature discharge, although negative ones are more difficult to produce and they typically arise in discharges in which electrons attach themselves to neutral molecules. A more detailed description of the production of negative ions will be given in the following subsection[1]

2. Extractor and Accelerator: The ions are extracted by an electrode system and then accelerated to higher energies by means of a high voltage, negative for positive ions and positive for negative ions

3. Neutralizer: A long tube filled with neutral particles. In this stage, the negative ions are neutralized by inelastic collisions like charge exchange reactions

4. Residual Ion Dump: It is based on a electrostatic deflector. This step is necessary because the output of the neutralizer contains both neutral particles and high-energy ions which escaped from the neutralization. This situation is undesirable because these ions carry a considerable amount of power and they could deposit their energy on the neutral beam entrance port. Thus, in this stage the high-energy ions are deflected and their energy is collected on the beam dump

The remaining neutral particles are then injected into the tokamak where they can deposit their energy in the background plasma.

1.4.2 Why Negative Ions?

Positive ion beam are easily produced in plasma sources. Unfortunately the neutralization efficiency of positive ions drops to 0 at the high energies requested by the new generation of high power NBI's, see Figure 1.7. Negative ions instead are more easily neutralized since the extra electron is weakly bound to its neutral atom so the neutralization efficiency remains almost constant with the energy of the particles. For this reason ITER NBI's are based on negative ion sources, despite the fact that H^-/D^- particles are more difficult to produce than positive H^+/D^+.

1.4.3 Production of negative ions

Two are the main processes for producing H^- or D^-:

[1]It is not possible to distinguish the negative ions from the electrons, so an intermediate magnetic grid is necessary in order to separate the electrons from the beam of ions

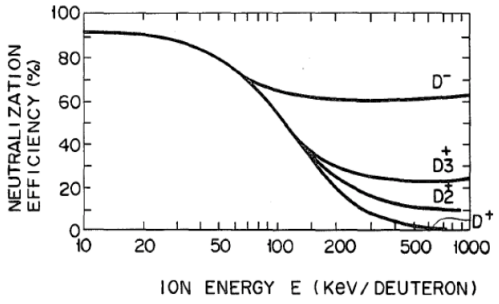

Figure 1.7: Neutralization efficiency for positive and negative ions [9]

Volume Production: A vibrationally excited hydrogen (or deuterium) molecule can capture a low energy electron through a process called *dissociative electron attachment*:

$$e^- + H_2(\nu'') \longrightarrow H(1s) + H^-$$

The process needs:

- One fast electron (high energy>10 eV) to produce the highly vibrationally excited hydrogen molecule.
- One slow electron to ensure the electron attachment.

Two process are dominant for the destruction of negative ions: the *electron stripping* ($e^- + H^- \longrightarrow 2e^- + H^0$) and the *mutual neutralization* ($H^+ + H^- \longrightarrow 2H^0$). Electron stripping can be minimized by reducing T_e to approximatively 2 eV, thus the source has to be divided into two parts: a hotter region, the *driver*, where the vibrationally excited H_2 molecule is produced and a colder region, *the extraction region*, where the H^- formation takes place. A magnetic filter allows to reduce the temperature of electrons diffusing from the driver (T_e>4 eV) to the extraction region (T_e<2 eV).

Surface Production: [2] Since the survival length for the negative ions is reduced by processes like the mutual neutralization, the negative ion formation close to the extraction system has to be maximized. This is achieved by a surface processes in which an electron at the Fermi level in the conduction band of a metal shifts by tunneling into a level of

[2] the 'trick' of this method is to use a thin layer of an elements of low work function deposited on the surface of a metal (usually the plasma grid of the extraction system). From [8] we can see that caesium has the lowest work function (1.81 eV)

an atom or molecule. An example of this process is performed with a caesiated wall which has low work function.

$$H^0 + Cs(wall) \longmapsto H^- + Cs(wall)$$

where H^0 fragments are produced by a two-step process involving H_2 excitation by electron impact followed by dissociation:

$$e^- + H_2(X, 0) \longrightarrow H_2^* + e^- \longrightarrow 2H^0 + e^-$$

Chapter 2

The NIO1 Experiment and Diagnostic Methods

NIO1 is a compact-versatile RF ion source commissioned by Consorzio RFX and INFN. The aim of the experiment is the production of a nominal beam current of 135 mA at -60 kV. The beam is divided into 9 beamlets (arranged in a 3×3 matrix).
The plasma source and the accelerating column for the H^- beam, shown in Figure 2.1, are contained in a 2 m long vacuum chamber including diagnostic ports and pumps. The production of this beam and the study of the parameters of the source is useful to understand the physics and technology of NBI's for future improvement [13] [12].

2.1 The Source

The source is a plasma-based compact cylinder of 98 mm diameter and 211.7 mm long where the plasma is formed by radiofrequency (2 MHz, 2500 W radiofrequency system made by 7 turn coils around the source wall) and confined magnetically. The magnetic confinement represents a minimum $|\vec{B}|$ configuration where the dense-central plasma is separated from the wall (magnetic bottle confinement). Two plasma regions can be identified:

1. The Driver: where the gas is dissociated and ionized. Here the electron temperature is high (typically $T_e \geq 4eV$)

2. The Extractor/Expansion Region: where the plasma cools by expansion or for the effect of a magnetic filter

NIO1 started its full operation in July 2014 using air as a filling gas. After a 4-months stop of the operations due to refurbishment of some components,

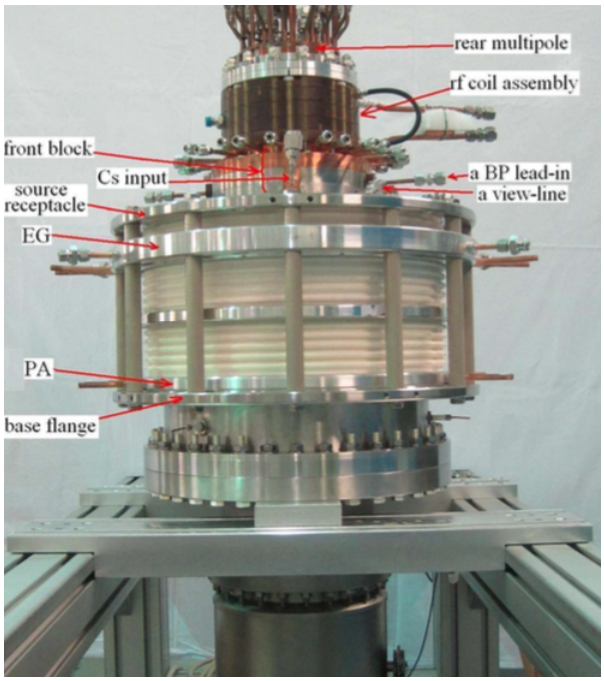

Figure 2.1: NIO1 source and accelerating system detail, from [11]

the use of Hydrogen has been implemented. A controlled valve injects the gas into the source, so the pressure of the source has to be monitored by a vacuum gauge. NIO1 is designed to include a caesium oven to allow surface production of H^-, but to avoid contamination it will not be used in the first year of operation.

2.2 The Acceleration System

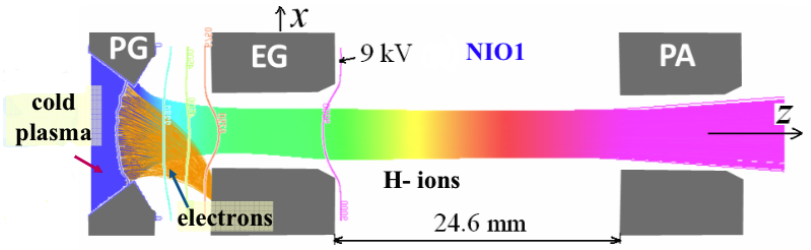

Figure 2.2: Simulation of ion beam and electron dump, from [10]

The acceleration system involves 3 acceleration grids, as shown in Figure 2.2 and Figure 2.3:

1. Plasma Grid (PG): It faces the plasma and it is essentially at the source voltage (-60 kV)
2. Extraction Grid (EG): It is at higher potential than PG ($V(EG) - V(PG) = 8kV$) to extract and accelerate negative ions. Here the co-extracted electrons are stopped by 4 permanent magnets inserted in the EG
3. Post Acceleration Grid (PA): It is set essentially at ground potential. After this grid there is a so called *Repeller Grid* used to repel positive ions that come from the region downstream of the repeller itself, generated by ionization of the background gas

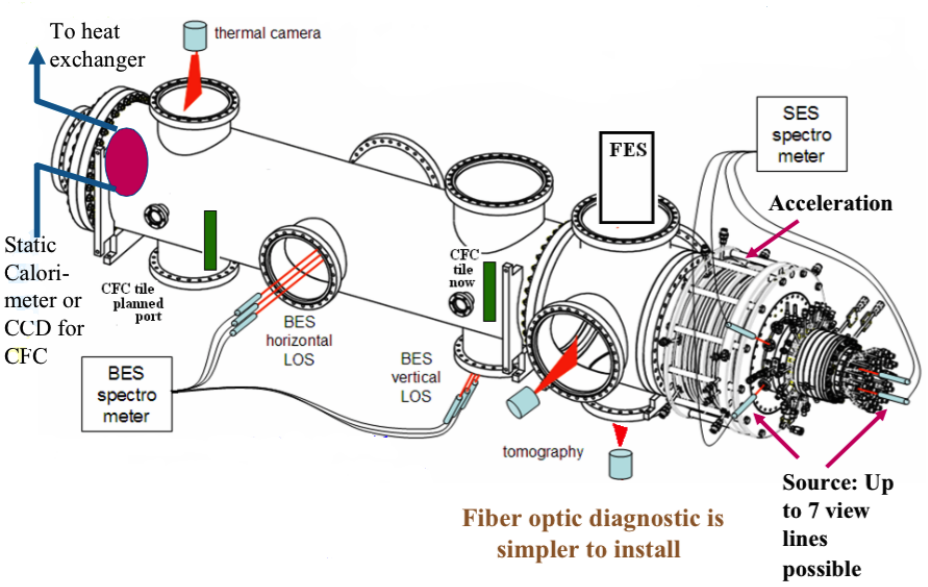

Figure 2.3: The NIO1 apparatus and diagnostics

After the acceleration, the beam drifts along the beam tube (84 mm internal diameter) and the diagnostic chamber (1.5 m long). NIO1 is not provided with a neutralizer, the beam is dumped onto a calorimeter used to determine the beam intensity profile.

2.3 NIO1 Diagnostics

The NIO1 Experiment is characterized by a full set of diagnostic systems (see Figure 2.4) capable of providing the main parameters of plasma source and accelerated beam [14]. The source could be investigated by:

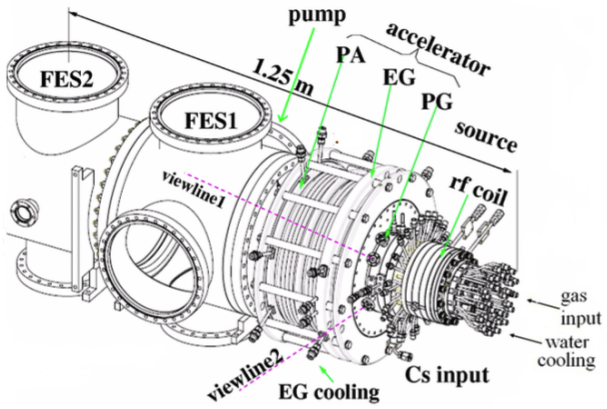

Figure 2.4: Overview of the source, accelerator and diagnostic chamber

Optical Emission Spectroscopy (OES): The radiation spontaneously emitted by atoms or molecules in the source is collected and analyzed in order to determine the main plasma parameters such as electron density and temperature.

Plasma Light Detection (PLD): It is used to investigate plasma ignition or fast plasma dynamics

Laser Absorption Diagnostic (LAD): It is useful to measure caesium density. The mechanism that underlies this process is based on the absorption spectrum of a laser with a set frequency on a resonant transition of atomic Cs.

Cavity Ring Down Spectroscopy (CRDS): It allows to measure the negative ion density.

The diagnostics that are soon-to-be implemented for the accelerated beam are:

Beam Emission Spectroscopy (BES): It will help to study the uniformity and divergence of the beam.

Fast Emittance Scanner: It provides measures of the beam particle distribution.

Visible Tomography: It is based on the H_α emission to measure the beam density profile.

Mini-STRIKE Calorimeter: A CFC tile is exposed perpendicularly to the beam and it is observed by a thermal camera in order to obtain information about the intensity profile

2.4 Experimental Setup

NIO1 is provided with several ports: some of them are placed in the diagnostic chamber, they are relatively big and arranged in opposite pairs. The ports located in the source are placed near the PG (Plasma Grid) at 26 mm from the plasma grid itself (8 mm aperture) and in the rear lid (12 mm aperture) in order to investigate the source. There are 4 LOSs (lines of sight): two of them parallel to the PG (26 mm from it) and two more perpendicular to the PG itself. The LOSs used for OES are shown in Figure 2.5.

OES collects the light emitted by the source plasma using optical heads placed on the smaller ports. An *optical head*, see Figure 2.6, conveys the light and consists in a cylinder (20 mm diameter, 104 mm length) that hosts a lens 50 mm of focal length. An *optical fiber* (400 μm core diameter) takes the signal to a spectrometer.

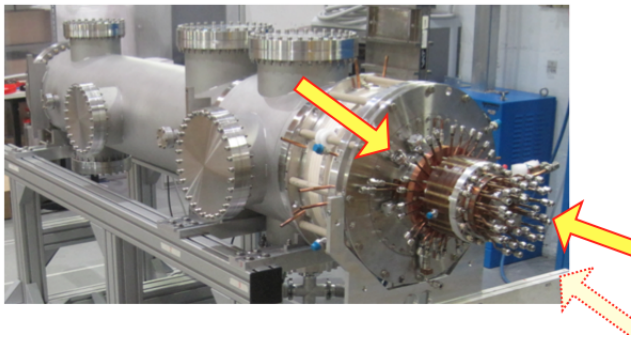

Figure 2.5: Lines of sight for OES

The two types of spectrometers used for OES are:

	Low Resolution	High Resolution
Type	Hamamatsu $C10082CAH$	Acton SpectraPro-750
Spectral Resolution	1 nm	0.05 nm
Spectral Window (of a single acquisition)	[200 : 850] nm	6 nm wide

The Low Resolution Spectrometer has an integrated CCD sensor of 2048 pixels, while the High Resolution Spectrometer[1] has a CCD camera of 512x512 pixels.

[1]this is a Czerny-Turner spectrometer (0.75 m focal length, grating of 1200 gr/mm) with two adjacent mirrors

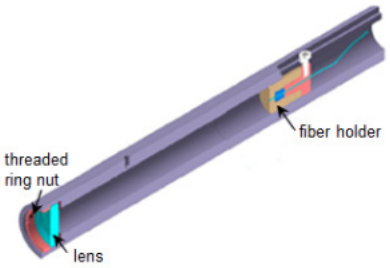

Figure 2.6: Optical Head

2.5 Theoretical Models

2.5.1 Measured Quantities

OES is a basic method to estimate plasma parameters by measuring the radiation spontaneously emitted by the source [32]. The plasma emits a quantity of energy via electromagnetic radiation per unit time, this quantity is called *radiative loss*. The *emission coefficient* (in $\mathrm{W\,m^{-3}\,sr^{-1}}$) is defined as : $\epsilon(r) = \frac{d^2\phi(r)}{dV d\Omega}$ where $d\phi$ is the *radiant flux* (in W) from the volume dV and over the solid angle $d\Omega$. In the same way, a quantity called *radiance*, see Figure 2.7, (in $\mathrm{W\,m^{-2}\,sr^{-1}}$) can be defined as the radiant flux per unit area ($\mathrm{dA}\cos\theta$) per solid angle ($\mathrm{d}\Omega$) as: $L = \frac{d^2\phi(r)}{dA\cos\theta d\Omega}$. In our case, a spectral line is emitted when an electron undergoes a transition from an upper level of energy to a lower one.

The main process involved is the excitation of atoms/molecules by electron impact from a lower level q to upper level p and the consequent decay into a level k by spontaneous emission. The conservation of energy gives the central wavelength of emission:

$$\lambda_0 = \frac{hc}{E_p - E_k}$$

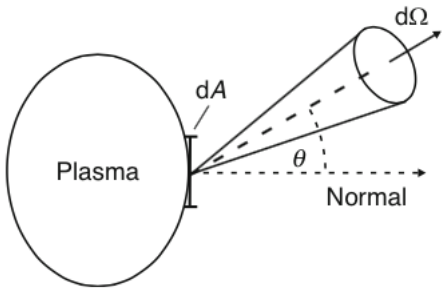

Figure 2.7: Visualization of radiance, from [25]

The total quantity of the radiant flux is called *line emission coefficient* and can be obtained by integrating the radiant flux $\epsilon_\lambda(\vec{r})$ over wavelength interval:

$$\epsilon_{pk} = \int_{los} \epsilon_\lambda d\lambda = n(p) A_{pk} \frac{hc}{4\pi\lambda_0}$$

where A_{pk} is an atomic constant dependent on the transition known as *transition probability* or *Einstein Coefficient* (in unit s^{-1}) and $n(p)$ is the population density of the excited level p. This relation combines the line intensity with the population density of the excited state. Although ϵ_{pk} is measured in $W\,m^{-3}\,sr^{-1}$, it's useful to define the *line radiation* or *emissivity* as:

$$I_{pk} = n(p)A_{pk}$$

(in $ph\,s^{-1}\,m^{-3}$).

2.5.2 Population Models

The population density of excited states depends on a variety of plasma parameters. The most important are: electron density (n_e), electron temperature (T_e) and the velocity distribution function of the particles[2]. By comparing the plasma emission measurements with the previsions of a population model, the plasma parameters can be derived. The model that can be applied depends on the equilibrium reached between collision and radiative processes in populating or depopulating the excited levels.

Thermodynamic Equilibrium This model is used to calculate the population density of excited states for high electron density ($n_e \geq 10^{24}m^{-3}$ for hydrogen plasmas) that are very effective to thermalize the states due to electron collisions. Intuitively, we can describe this situation as a plasma confined in a box with a constant temperature T. The properties of this model are:

- The energy distribution function of each particles is a classical Maxwell-Boltzmann distribution
- The radiation energy is given by Planck's law

Most plasmas, however, are not in thermal equilibrium. Radiation usually escapes from plasmas, thus the radiation fields inside the plasma is below Planckian radiant energy density. Nevertheless, at high densities, collisions will be so frequent that they maintain steady-state population densities according to the Boltzmann law. These conditions represent the concept known as *local thermodynamic equilibrium* (LTE).

Corona Model This model acquired its name from solar corona where n_e is low ($\sim 10^{12}m^{-3}$) and T_e is high ($\sim 100eV$). At low densities, collision processes become very weak compared to radiative ones. This model

[2]The velocity distribution function is Maxwellian if collisions are dominant

describes depopulation of excited levels only by radiative decay and population processes by electron collisions.

Collisional-Radiative Model (CR model) This model balances collisional and radiative processes. It is suitable for intermediate electron density and temperature ($10^{16}\mathrm{m}^{-3} \leq n_e \leq 10^{24}\mathrm{m}^{-3}$ and $1eV \leq T_e \leq 10eV$ for hydrogen plasmas).

The typical processes considered in a population model are:

Electron Impact Excitation: $a + e_f \longrightarrow a* + e_s$

Electron Impact de-excitation: $a* + e_f \longrightarrow a + e_s$

Spontaneous Emission: $a + h\nu \longleftarrow a*$

Electron Impact Ionization: $a + e_f \longrightarrow i + e + e_s$

Radiative Recombination: $a + h\nu \longleftarrow i + e$

(Three Body) Radiative Recombination: $i + e + e \longrightarrow a + e$

where a and i are the atom and the ion in the ground state, a^* is the excited atom, e_f and e_s describe the fast and slow electron respectively, e is the electron irrespective of its speed.
As seen before, the emissivity is proportional to the population density of excited levels: $I_{pk} = n(p)A_{pk}$. If each process is described by its probability, the time development of the population density of state p is given by:

$$\frac{dn(p)}{dt} = \underbrace{\sum_{k<p} n(k)n_e X^{exc}_{k,p} + \sum_{k>p} n(k)n_e X^{de-exc}_{k,p}}_{\textit{populating processes by } e^- \textit{-impact from } k \neq p}$$

$$\underbrace{- \sum_{k<p} n(p)n_e X^{de-exc}_{p,k} - \sum_{k>p} n(p)n_e X^{exc}_{p,k} +}_{\textit{depopulating processes}}$$

$$\underbrace{- \sum_{k<p} n(p)A_{p,k} + \sum_{k>p} n(k)A_{k,p}}_{\textit{spontaneous emission from and into state } p} \quad \underbrace{-n(p)n_e S_p + n_e n_e n_i \beta_p + n_e n_i \alpha_p}_{\textit{ionization and recombination}}$$

Where α_p and β_p are the so-called *rate coefficients* for three-body and radiative recombination respectively, S_p is the rate coefficient for ionization of the state p, $X^{exc/de-exc}$ are the so-called rate coefficients for electron impact

excitation/de-excitation. In case of binary collisions, the rate coefficient is written as:

$$X^{exc} =< \sigma v >= \int_{\vec{v_1},\vec{v_2}} \sigma(v) v f_1(\vec{v_1}) f_2(\vec{v_2}) d^3\vec{v_1} d^3\vec{v_2}$$

and can be expressed in $\mathrm{m}^3\,\mathrm{s}^{-1}$. $\sigma(v)$ is the *cross section* of the process and f_1 and f_2 are Maxwellian at temperature T. Since in atomic systems the times to reach steady-state population for an excited level p are typically very short compared to changes of plasma conditions, usually the approximation of $dn(p)/dt = 0$ is adopted. The solutions of these equations can be written as:

$$n(p) = R_0(p) n_0 n_e + R_i(p) n_i n_e$$

where n_i is the ionic population, n_0 is the ground state population, $R_0(p)$ and $R_i(p)$ are the *coupling coefficients* (or *population coefficients*) for ground state and ionic processes. In most cases recombination can be neglected, thus the coupling to the ion can be neglected. Considering the precedent formulas, it is easy to see that the emissivity (or line radiation) can be written as:

$$I_{pk} = n_0 n_e X_{pk}^{eff}(T_e, n_e)$$

where $X_{pk}^{eff} = R_0(p) A_{pk}$ is the *effective emission rate coefficient* depending on plasma parameters.

2.5.3 CR Model for the Hydrogen Atoms and Molecules

The CR model used in this thesis is the YACORA model developed at IPP Garching [29] [30]. When applied to H or D, it gives the rate coefficients as a function of electron temperatures and densities. The population density of an excited state of atomic hydrogen, coupled to 6 other species.

The reactions considered are:

Electron Impact Excitation: $H(q) + e^- \longrightarrow H(p > q) + e^-$

Electron Impact De-excitation: $H(q) + e^- \longrightarrow H(p < q) + e^-$

Spontaneous Emission: $H(q) \longrightarrow H(p < q) + h\nu$

Ionization: $H(q) + e^- \longrightarrow H^+ + 2e^-$

Recombination of H^+: $H^+ + 2e^- \longrightarrow H(p) + e^-$

Recombination of H^+: $H^+ + e^- \longrightarrow H(p) + h\nu$

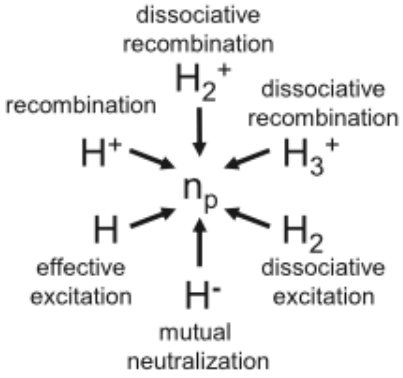

Figure 2.8: The 6 species coupled with H in the CR model

Dissociation of H_2: $H_2 + e^- \longrightarrow H(p) + H(1) + e^-$

Dissociation of H_2^+: $H_2^+ + e^- \longrightarrow H(p) + H^+ + e^-$

Dissociative Recombination of H_2^+: $H_2^+ + e^- \longrightarrow H(p) + H(1)$

Dissociative Recombination of H_3^+: $H_3^+ + e^- \longrightarrow H(p) + H_2$

Mutual Neutralization: $H_x^+ + H^- \longrightarrow H(p) + H(1)$

In most cases, *opacity* (i.e. self absorption) may be also important.
The vibrational and rotational states of the molecules influence the reactions' cross sections and have to be taken into account.
The molecules are described with additional quantum numbers due to vibrational and rotational motions, these are ν (or w) and J respectively. Energy levels are often described with upper and lower case letters, where X refers to ground state. The reactions to the rotovibrational state of H_2 molecules are:

Electron Excitation: $H_2(\nu) + e^- \longrightarrow H_2^- \longrightarrow H_2(w \neq \nu) + e^-$

Dissociation: $H_2(\nu) + e^- \longrightarrow H_2(b) + e^- \longrightarrow H + H + e^-$

Ion Conversion: $H_2(\nu) + H^+ \longrightarrow H_2^+ + H$

Dissociative Attachment: $H_2(\nu) + e^- \longrightarrow H_2^- \longrightarrow H^- + H$

The model could be extended with electron-impact excitation followed by radiative decay or heavy particle collision (for example: $H_2 - H_2$ collision). In Chapter 4, the experimental emissivities of NIO1 source plasma will be interpreted by the prevision of YACORA model, in order to determine T_e, n_e and the dissociation degree (n_H/n_{H_2}).

Chapter 3

Measurements in Air

In this part of the thesis, the analysis on the emission spectra of the NIO1 source when air was used as filling gas is presented. In particular it was possible to determine electron temperature (T_e), vibrational temperature (T_v) and rotational temperature (T_r) and to study the dependence of these parameters on the filling pressure and RF power [23]. According to [13], the choice of using air as a filling gas has been made for producing an intense beam even without the contribution of caesium oven, because of electronegativity of oxygen atoms. The analysis was performed with codes written in IDL (Interactive Data Language) [18].

3.1 Electron Temperature

By comparing the emission of neutral and ionized N_2 molecules it is possible to estimate the electron temperature. A theoretical model was developed by A.Ricard [23] based on corona model. According to this model, the band head intensity ratio of the molecular band $N_2^+(B, 0-X, 0)$ at 391.4 nm and $N_2(C, 2-B, S)$ at 394.3 nm ($R = \frac{I(391.4nm)}{I(394.3nm)}$) has a strong dependence on T_e, as shown in Figure 3.1.

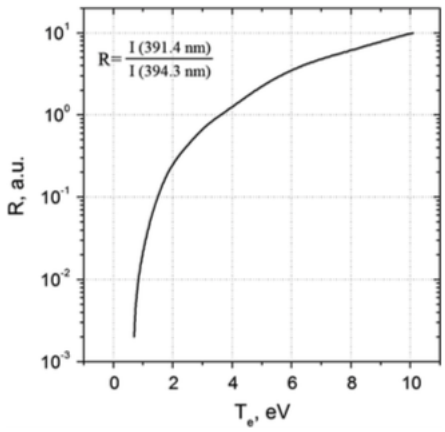

Figure 3.1: Intensities Ratio (R) as a function of electron temperature (T_e)

This model can be used when the following conditions are fulfilled:

1. The EEDF is assumed to follow a Maxwellian distribution function.[1]

2. The electron states of N_2 and N_2^+ are mainly excited by electron impact collisions from ground state. This condition generally takes place in discharges at low gas pressure.

3.1.1 Analysis Method

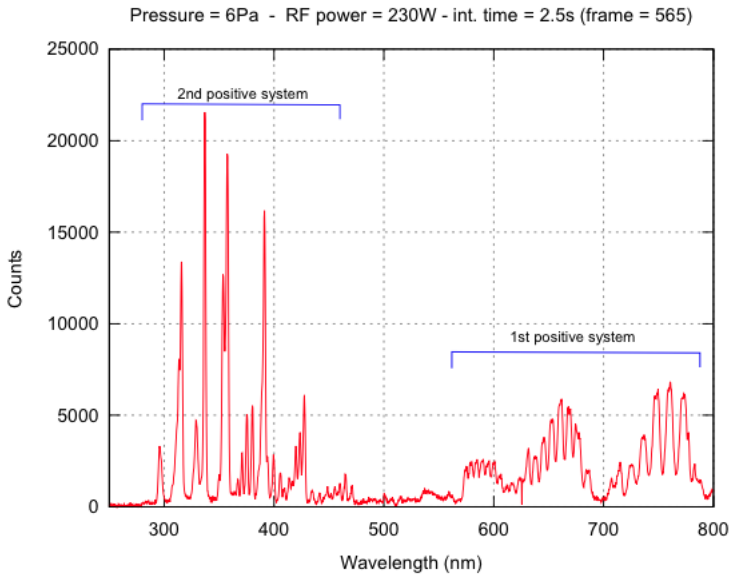

Figure 3.2: Spectrum acquired with the low resolution spectrometer. Air was used as filling gas

The spectra of air discharges are dominated by the nitrogen and oxygen emissions, in particular by the *roto-vibrational bands* of N_2 as shown in Figure 3.2. The measurements were taken by low and high resolution spectrometers upon varying the RF power and the gas pressure. For the low resolution spectrometer, the exposure time ranges from 1 s to 6 s according to

[1]Electrons are energy providers for many plasma processes. The rate of such processes depends on the number of electrons having sufficient energy: this is described by the EEDF, which is a probability density for an electron to have the energy E. When the EEDF depends mostly on T_e, it can be defined by the $Maxwell-Boltzamann$ distribution function. Quite often this distribution function strongly depends upon the electric field and gas composition, and can be very far from the *M.-B.* distribution.

the signal level. The long exposure times required a careful background subtraction: dark frames with the same exposure times as the acquired spectra have been also collected in order to be subtracted. Also for each experimental condition several identical spectra have been acquired and averaged for reducing the noise. Using a code developed in IDL, the intensities of the two molecular bands at 391.4 nm and 394.3 nm have been obtained. A multi-gaussian fit gave the best results especially in the case of overlapping lines, although the shapes of the peaks are not gaussian because of the rotational bands at shorter wavelengths. An example of double gaussian fit is shown in Figure 3.3, while in Figure 3.4 the same peaks are shown, but taken with an higher spectral resolution.

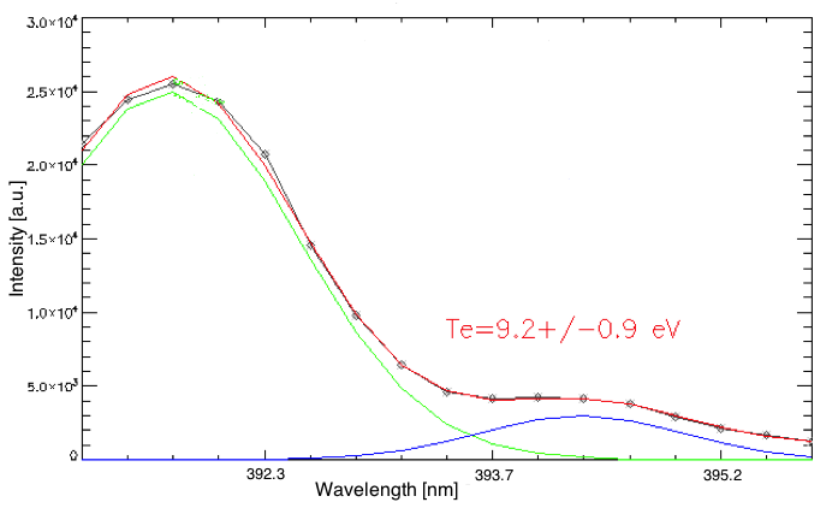

Figure 3.3: Double gaussian fit of N_2^+ 391.4 nm and N_2 394.3 nm. Data were acquired by the low resolution spectrometer. The intensities ratio and the estimated T_e are also reported in the graph

From the intensities ratio of the two bands, using the dependence shown in Figure 3.1, the corresponding T_e has been obtained. An error has been associated to T_e given by the variation of 10% of the intensities of 391.4 nm and 394.3 nm, according to the following formula:

$$\sigma(T_e) = \max(|T_{e,sup} - T_e|, |T_e - T_{e,inf}|)$$

where $T_{e,inf}$ is derived from $R_{inf} = \frac{I(391.4nm) - 10\% \cdot I(391.4nm)}{I(394.3nm) + 10\% \cdot I(394.3nm)}$ and $T_{e,sup}$ from $R_{sup} = \frac{I(391.4nm) + 10\% \cdot I(391.4nm)}{I(394.3nm) - 10\% \cdot I(394.3nm)}$.

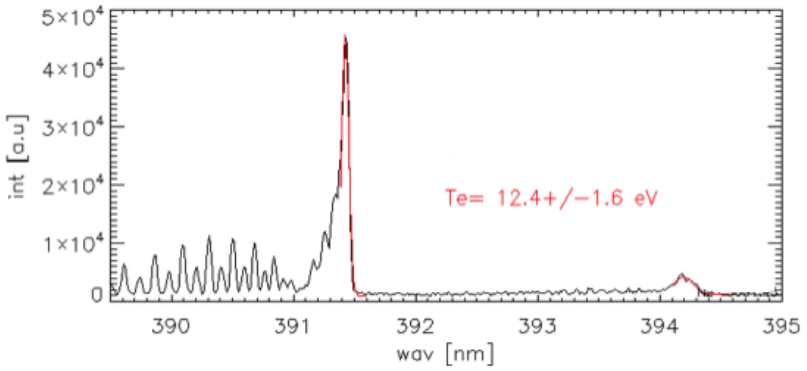

Figure 3.4: Double gaussian fit of N_2^+ 391.4 nm and N_2 394.3 nm. Data were acquired by the high resolution spectrometer. The intensities ratio and the estimated T_e are also reported in the graph

3.1.2 Results and Comments

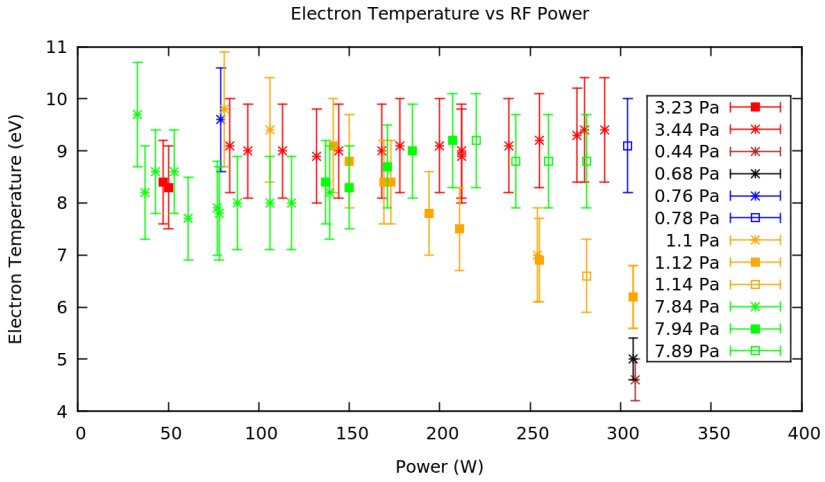

Figure 3.5: Electron Temperature in function of power, low resolution spectrometer, filling pressure in the range 0.68:7.94 Pa

The estimations of T_e obtained from the measurements taken with the low resolution spectrometer are shown in Figure 3.5 where T_e is reported as a function of RF power and filling pressure. Analogously, Figure 3.6 shows the estimates of T_e derived by measurements with high resolution spectrometer. The differences between the estimates of T_e with low and high resolution spectrometers indicate that this method has to be improved.

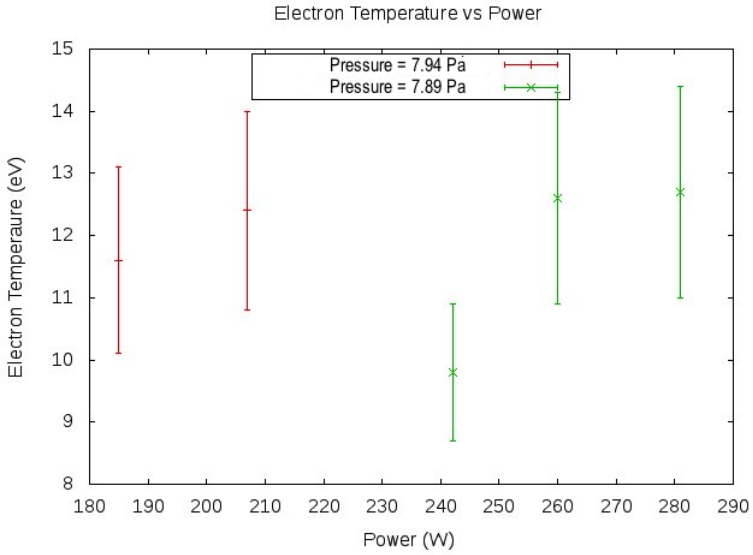

Figure 3.6: Electron Temperature in function of power, high resolution spectrometer, filling pressure about 7.9 Pa

According to [23], Figure 3.5 shows that T_e does not depend on the applied RF power in the range 50-300 W for filling pressures in the range 3.9÷7.9 Pa. On the other hand, for filling pressure between 1.1 Pa and 1.14 Pa, T_e seems to decrease with the applied RF power. This result may be due to the fact that the corona model is not valid and has to be substituted with a more appropriate CR model that includes ionization processes. Even if for heavy particles the Maxwellian EEDF can be used, this distribution can deviate from a Maxwellian one since electrons make inelastic collisions.[2] The type of EEDF assumed in this case is the *Druyvesteyn distribution*, as suggested in [26]. Intuitively, in this range of low RF power ($50 \div 300$ W), the electrons are accelerated by the power transferred via RF inductive coupling and they slow down into the source and give up their energy to the molecules or other atoms that are excited by electron impacts. Thus, in this experimental range, the molecular excitation is due to the 'tails' of faster electrons that cause the radiation emissions. This is probably the cause of the higher values of T_e estimated in this analysis than the ones predicted in [16].

[2] *Elastic collisions* are those in which the internal energy of colliding particles does not change and the total kinetic energy is conserved. Otherwise, *inelastic collisions* determine transfer of energy from kinetic into internal energy. Examples of inelastic collisions are ionization and excitation of molecules by electron impact

3.2 Vibrational Temperature

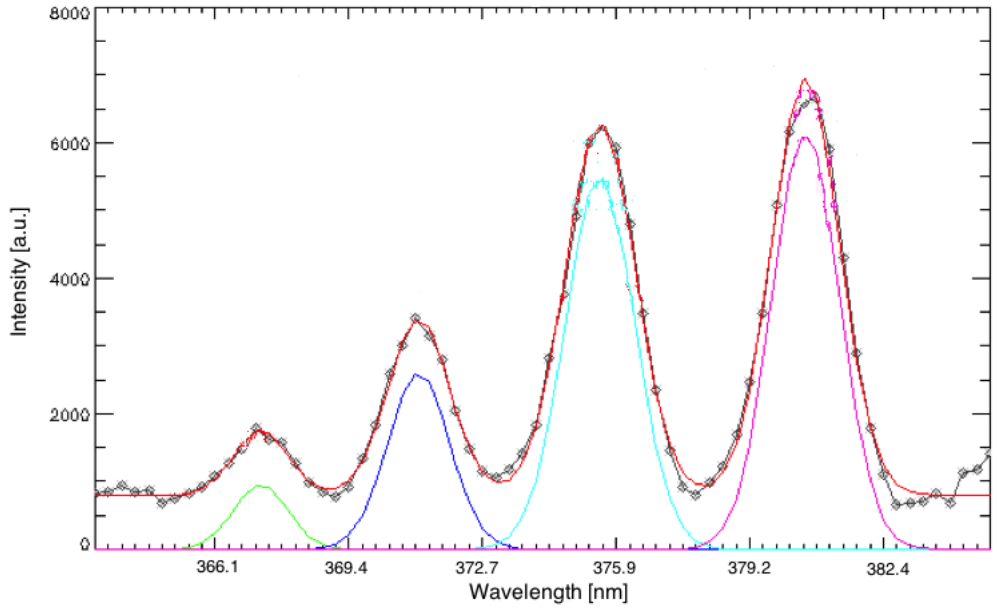

Figure 3.7: The second positive system of N_2 used to determine the T_v

Vibrational temperature (T_v) determines the population density of the vibrationally excited molecular bands. The vibrationally excited molecules play a key role in enhancing the reactivity of the plasma because vibrational excitation can trap energy and behave like a reservoir for chemical reactions inside the plasma.

3.2.1 Analysis Method

Figure 3.7 shows a particular of the second positive system of N_2 emission spectra between 365-383 nm. This spectral region comprises the band emissions relative to $\Delta\nu = -2$ transitions ((3-5) at 367.2 nm; (2-4) at 371.0 nm; (1-3) at 375.5 nm and (0-2) at 380.5 nm), used to determine the T_v. The bands appear in the spectra as a sequence of four peaks.
Assuming Boltzmann distribution for the population of vibrational levels, the ratio of the band head intensities at 367.2 nm, 371.0 nm, 375.5 nm with respect to the one at 380.5 nm was computed. Figure 3.8 shows the so-called *Boltzamann graph* where the dependence of the intensity ratio (in log-scale) with the corresponding vibrational quantum number ν' is highlighted.

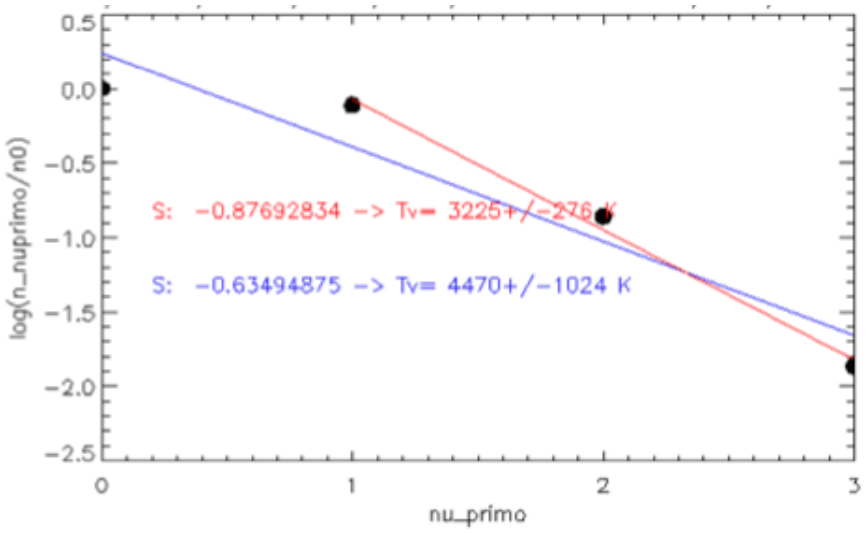

Figure 3.8: An example of Boltzamann graph

In this plot, the slope (S) is related to the vibrational temperature (T_v) by the following equation, derived from [23]:

$$T_v[K] = \frac{10^4}{3.57 \cdot S - 0.03}$$

As shown in Figure 3.8, the blue line is a fit considering the 4 ratios of aforementioned intensities, while the red one is another fit excluding the first point to the left which deviates from the linear trend. The errors of T_v were calculated with the following propagation formula: $\sigma_{T_v} = \frac{3.57 \cdot 10^4 \cdot \sigma_S}{(3.57 \cdot S - 0.03)^2}$ where σ_S is the error of the fit.

3.2.2 Results and Comments

In the present subsection, the estimates of T_v obtained from the measurements of low and high resolution spectrometers are presented. In particular, the dependence of T_v on RF power is outlined in the following graphs (Figure 3.9 and Figure 3.10). From this analysis, T_v seems to increase with RF power, more rapidly until 100/125 W and then saturate.

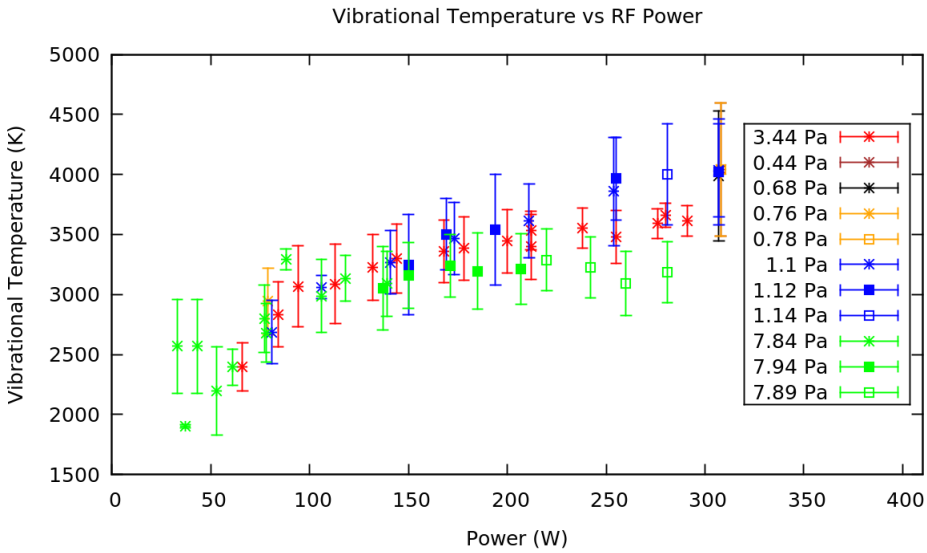

Figure 3.9: Vibrational temperature in function of power, low resolution spectrometer, filling pressure between 0.44 and 7.94 Pa

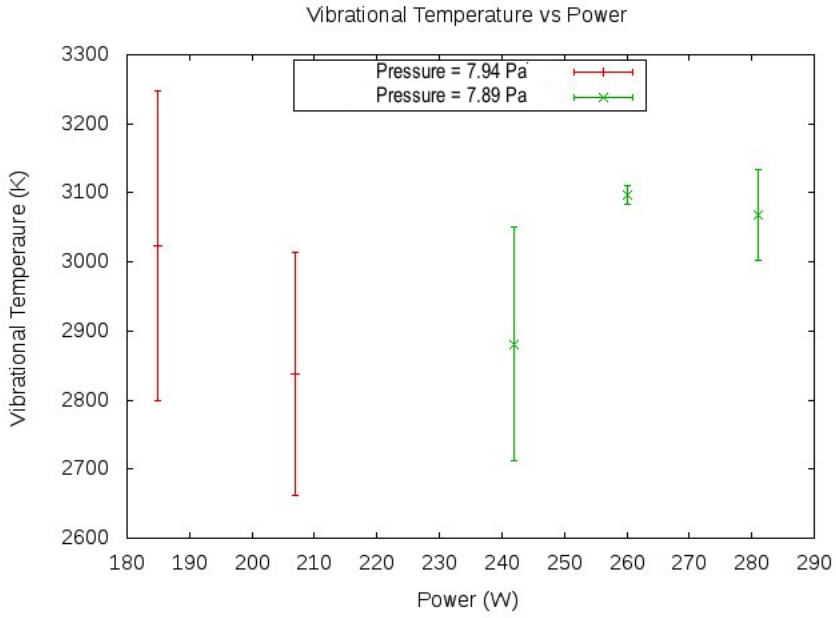

Figure 3.10: Vibrational temperature in function of power, high resolution spectrometer, filling pressure of 7.9 Pa

3.3 Rotational Temperature

The rotational temperature T_r of molecular species is said to be an indicator of neutral gas kinetic temperature (T_g) if the population originates only from heavy particles collisions.

3.3.1 Analysis Method and Results

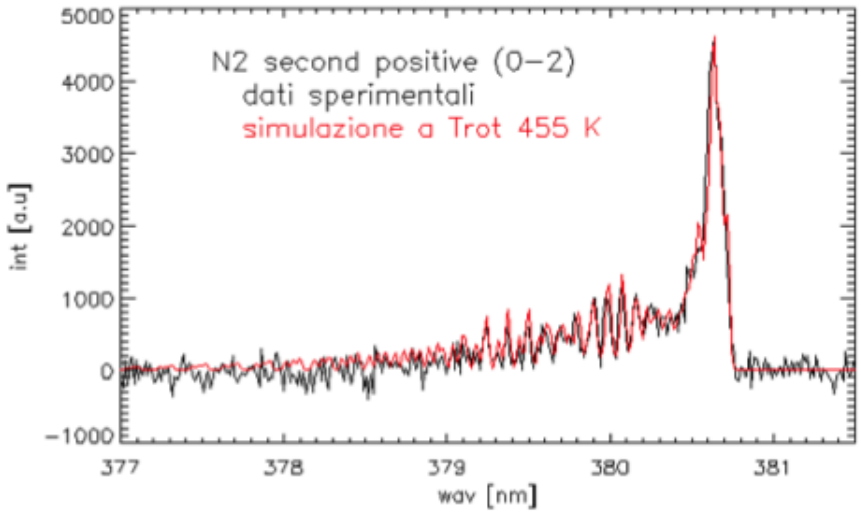

Figure 3.11: Spectrum collected with the high resolution spectrometer with superimposed simulation (red line) that better reproduces the experimental data. The value of T_r at which there is the best mach between the data and the simulation is also reported in the picture

Because of the small energy separation of the rotational levels, only high resolution spectrometer could be utilized for the determination of T_r. The analysis of (0-2) transition is shown in Figure 3.11 where a computer simulation of the spectra has been utilized with T_r as a parameter. This procedure considers the band of the (0-2) transitions of the second positive system and the variances between data and simulated spectra were performed with different rotational temperatures. Like a $\chi^{(2)}$ procedure, the 'parabola-like' curve of variances were cut at 5% above the minimum. It gives also an estimates (or confidence interval) of the errors of the rotational temperatures. The rotational temperatures obtained with this method are shown in the Figure 3.12. These results, with the ones previously obtained, demonstrate the classic inequality: $T_e > T_v > T_r$.

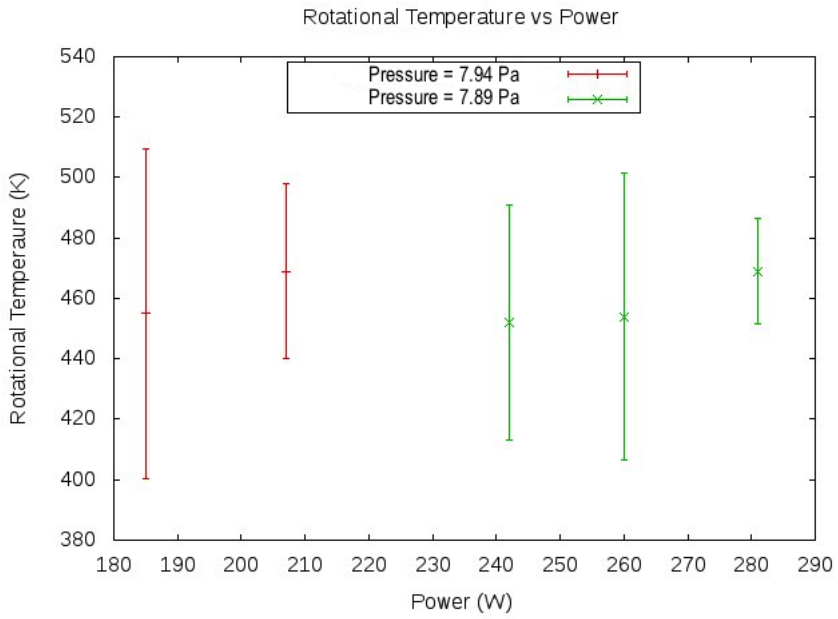

Figure 3.12: The estimates of T_r in function of RF power for filling pressure of about 7.9 Pa

Chapter 4

Measurements in Hydrogen

Optical emission spectroscopy (OES) of the hydrogen emission spectrum of NIO1 source is carried out to obtain line-of-sight averaged plasma parameters such as electron density (n_e), dissociation degree (n_H/n_{H_2}) and electron temperature (T_e) in different experimental conditions. An example of NIO1 source spectrum acquired by the low resolution spectrometer with 5 s of exposure time and input RF power of 340 W is shown in Figure 4.1.

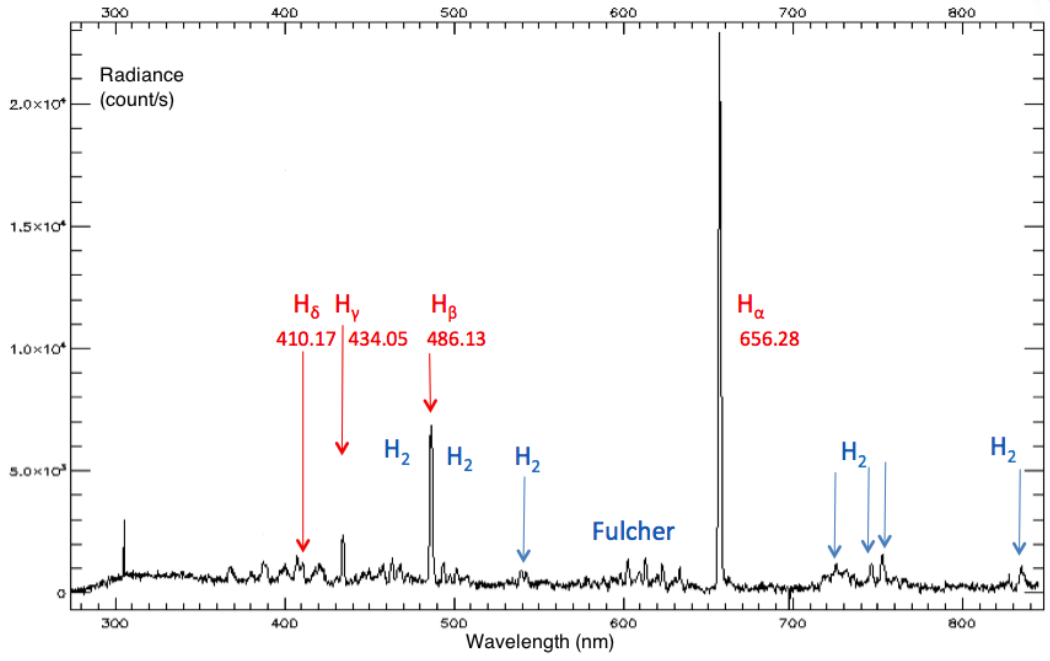

Figure 4.1: Spectrum recorded by low resolution spectrometer, in count/s. The source had an internal pressure of 2.5 Pa and an RF power 340 W. The exposure time was 5 s

The main visible emissions are:

- The Balmer lines: H_α transition ($3 \rightarrow 2$) at 656.28 nm, H_β transition ($4 \rightarrow 2$) at 486.13 nm, H_γ transition ($5 \rightarrow 2$) at 434.05 nm, H_δ transition ($6 \rightarrow 2$) at 410.17 nm
- The molecular H_2 emission: in particular the *Fulcher band* ($d^3\Pi_u \rightarrow a^3\Sigma_g^+$) mostly in the range 590:640 nm

By comparing the Balmer and Fulcher line emissivities with the predictions of YACORA, the Collisional-Radiative (CR) Model, the main plasma parameters could be deduced.
The spectrographic systems have to be absolutely calibrated in order to obtain the signal in radiance units (i.e. $\mathrm{ph\,s^{-1}\,m^{-2}}$)[1].

4.1 Line Fitting Methods

For the determination of plasma parameters, the radiances (in $\mathrm{ph\,s^{-1}\,m^{-2}}$) of a selection of lines have to be extracted from the acquired spectra. It will be seen in the following that the lines better suited for the analysis are: H_β, H_γ and $H_{2,Fulch}$. Different procedures of line fitting have been applied to the experimental spectra and give comparable results. These methods will be described in the next paragraphs.

4.1.1 The method of the sums

The easiest way to calculate radiances is simply to integrate the signal in the wavelength interval covered by the line profile. The following table reports these intervals for the lines of interest.

Transition considered	Spectral wavelength interval (nm)
H_β	[484 : 490]
H_γ	[432 : 437]
$H_{2,Fulch}$	[590 : 640]

Looking at Figure 4.2 and Figure 4.3, it can ben noticed that the spectra line sits above a *'continuum'* that has to be removed from the line integral. This continuum has two origins: the first is related to the CCD detector (bias, dark current etc.) and can be subtracted by acquiring a spectrum

[1]The absolute calibration uses an Ulbricht sphere as a reference sample, and converts the counts per second given by the CCD into photons per unit area per unit time ($\mathrm{ph\,s^{-1}\,m^{-2}}$)

at the same experimental conditions but without plasma light (background spectrum $b(x_i)$), the second one is more tricky because it consists of the continuum emission of the plasma itself. The solution adopted is to identify a nearby spectral region relatively free of lines and use its signal level ($F(x_i)$) as a measure of the continuum to be subtracted from the line integral.

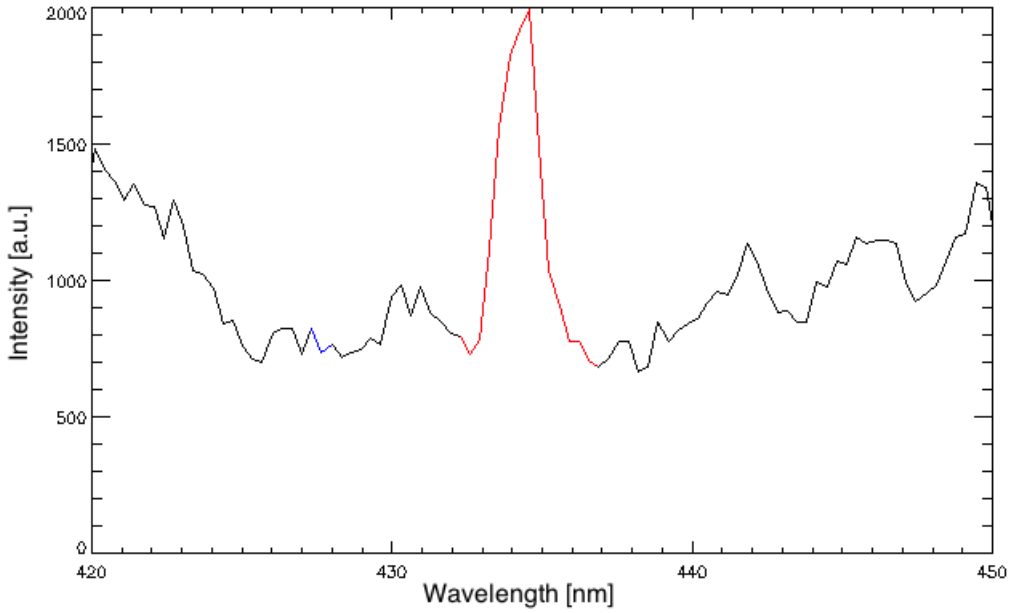

Figure 4.2: Spectrum recorded by low resolution spectrometer. The source had an internal pressure of 2.4 Pa and an RF power 1100 W. The exposure time was 2 s

If $f(x_i)$ is the acquired spectrum, x_i is the wavelength coordinate that can be expressed as a function of $\lambda(nm)$ or of the CCD pixel number p, $b(x_i)$ is the background spectra, the radiance I can be written as a sum over the spectral interval Δx relative to the transitions which can be expressed in pixel or nm[2]:

$$I = \sum_{i=i_1}^{i_2} [f(x_i) - b(x_i) - F(x_i)] \cdot \Delta x$$

Figure 4.2 shows an H_γ line acquired with the low resolution spectrometer at 1100 W of RF power, 2.4 Pa of source internal pressure and 2 s of exposure time. Looking at the Figure 4.2, the red curve represents the part of the

[2]In this analysis x_i has been considered in pixel and a spatial calibration performed with a Cd lamp allows to assign the wavelength to the correspondent pixel index

spectrum that has been integrated, while the blue curve corresponds to the part of the spectrum used for calculating F.
This method can be applied only if there are no overlapping lines. Also a bad choice of the spectral range of $F(x_i)$ can cause losses of signal and affects the estimations of the radiances.

4.1.2 The gaussian fit method

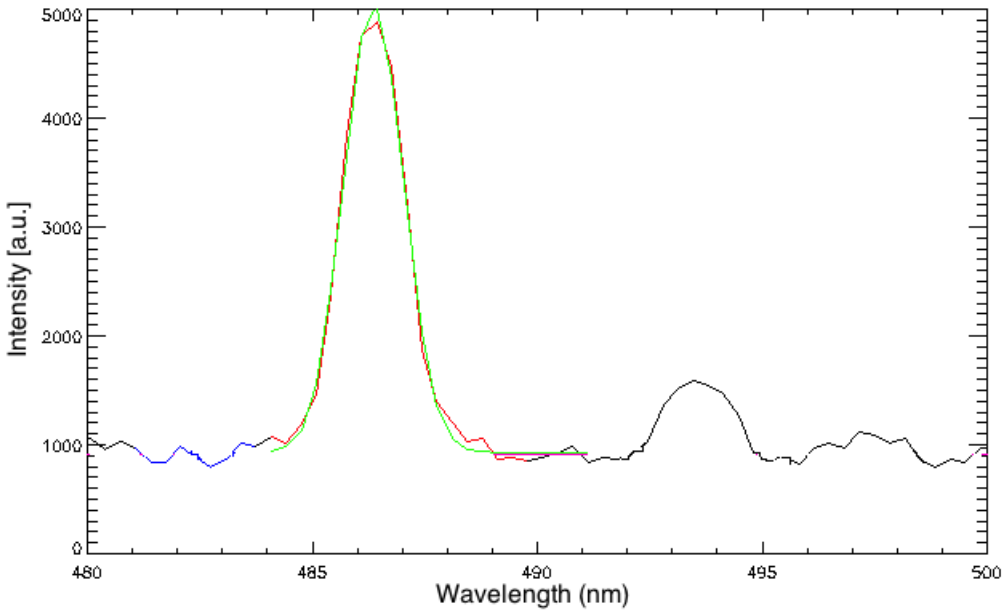

Figure 4.3: Spectrum recorded by low resolution spectrometer. The source had an internal pressure of 2.4 Pa and an RF power 898 W. The exposure time was 3 s

Another possible method consists in performing a gaussian fit of the line profile. This method has been implemented in order to calculate the radiances for H_β and H_γ lines because they typically present a bell-shaped profile, which can be approximated with a Gaussian curve[3]. Traditionally

[3]The atomic line broadening is mainly due to the following three phenomena: the *natural broadening* due to spontaneous emission which gives a lorentzian profile and it is described by the QED; the *Doppler broadening* due to the thermal motion of the atoms which gives a gaussian profiles; the broadening due to *atomic collisions* between the atoms and the background gas which gives a lorentzian shape. Typically the Doppler broadening gives the largest contribution, thus the lines in the visible range are often described with a gaussian profile although a mathematical approach gives a Voight profile [20] [21]

the gaussian fit of a spectral line parametrizes the gaussian curve with its peak, its centroid and its width at half its height (FWHM). Thus, the line integral is defined as:

$$I = FWHM \cdot peak \cdot \sqrt{\frac{\pi}{ln16}}$$

where *peak* is the gaussian peak and $\sqrt{\frac{\pi}{ln16}}$ is almost equal to 1.064 which come from calculation of the gaussian profile [22]. Figure 4.3 shows a H_β transition and the correspondent gaussian fit from a spectrum acquired with the low resolution spectrometer at 898 W RF power, 2.4 Pa filling source pressure and 3 s exposure time. The error of the acquired signal has two main contributions:

1. The Poisson statistics of the photons collected during the exposure time gives an error that depends on the square of the acquired signal
2. The conversion photons-counts of the ADC (Analog to Digital Converter) gives an error that depends only on the ADC sampling rate

The errors of the radiances were computed considering the following formula due to the gaussian fit:

$$\sigma_I = 1.064 \cdot \sqrt{(FWHM)^2 \cdot \sigma^2_{peak} + (peak)^2 \cdot \sigma^2_{FWHM}}$$

Figure 4.4 shows the calculated radiances of H_β transition and the corresponding errors as functions of the RF power for a filling pressure of 2.4 Pa. The results shows that the radiance increases with increasing power and there is a steep growth from 1300÷1400 W. This can be considered the condition at which E-H transition takes place (transition from capacitive to inductive coupling).
The radiances of H_γ, $H_{2,Fulch}$ are shown in Figure 4.5 as functions of RF power for a filling pressure of 2.4 Pa. As discussed more in details in Section 4.3, Figure 4.5 shows that the $H_{2,Fulch}$ emission seems to increase more rapidly than H_γ emission for higher values of RF power.

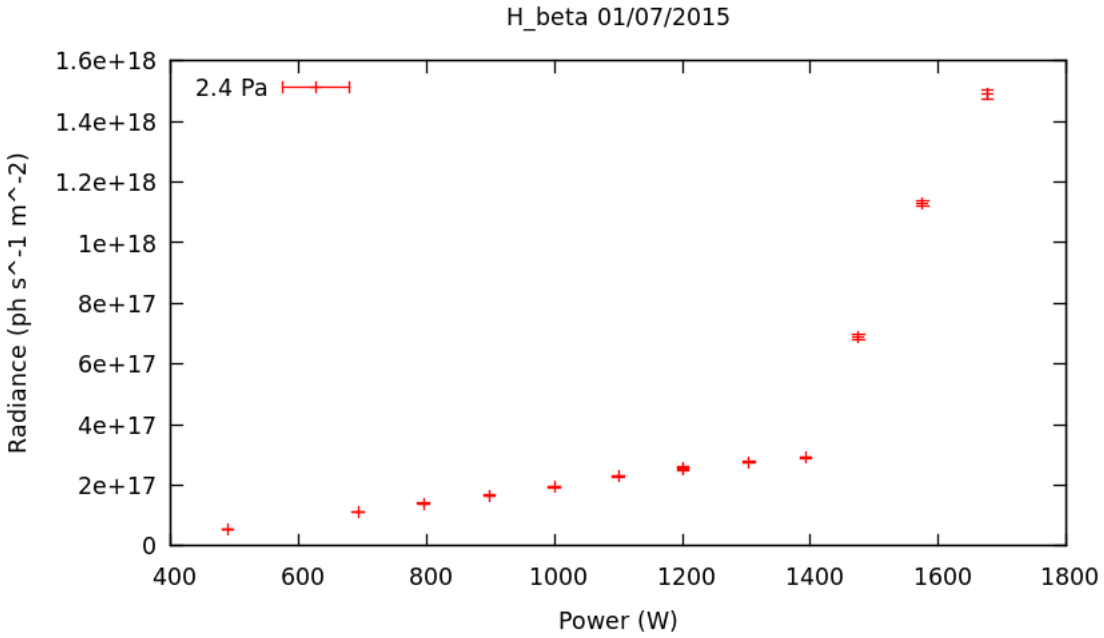

Figure 4.4: Radiance of H_β transition in function of power. From a spectra taken by low resolution spectrometer and filling pressure of 2.4 Pa

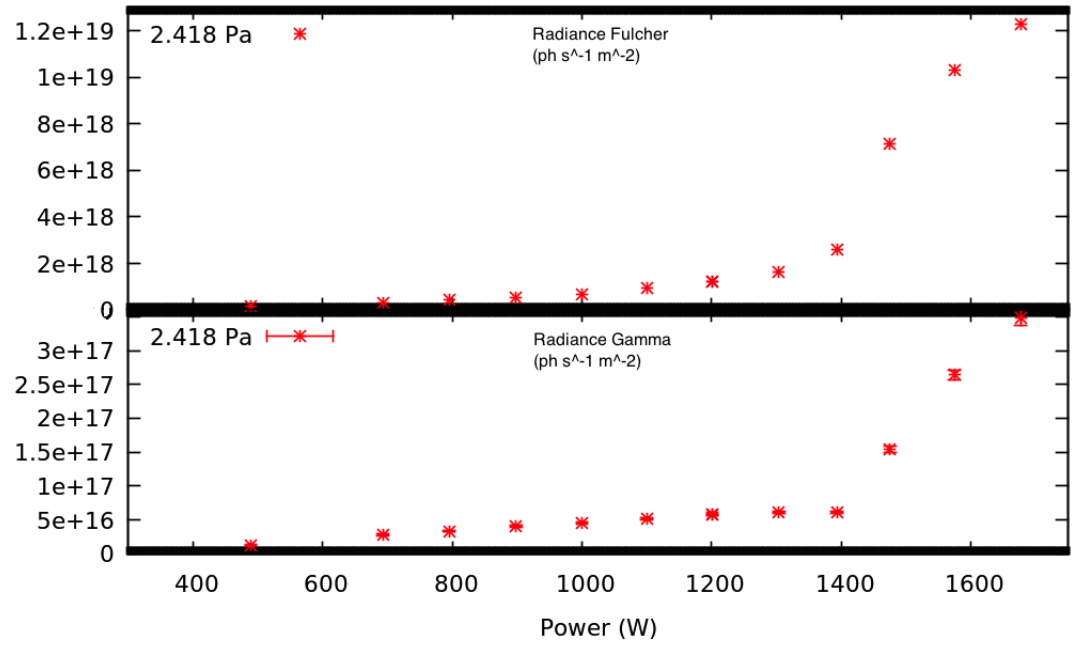

Figure 4.5: Radiance of H_γ (at the top) and $H_{2,Fulch}$ (at the bottom) transitions as a functions of power. From a spectra taken by low resolution spectrometer and filling pressure of 2.4 Pa

4.2 Electron Density

4.2.1 The Balmer line ratio

Assuming that the plasma emits the radiation isotropically and homogeneously, it is possible to deduce the experimental emissivities ϵ_{H_β}, ϵ_{H_γ} (in $\mathrm{ph\,s^{-1}\,m^{-3}}$) by dividing the radiances previously estimated by the length of the LOS ($L \sim 10\mathrm{cm}$). Detailed parameter studies [30] show that the method of comparing the ratio of experimental emissivities of H_β and H_γ with the values predicted by the CR model is well suited to obtain the plasma density in the range $1 \cdot 10^{17} \div 1 \cdot 10^{18}\ m^{-3}$.
According to Chapter 1, let n_e be the electron density, T_e the electron temperature, n_0 the particle density and X_{pk}^{eff} the effective emission rate coefficient given by the CR model and equal to the product of the population coefficient ($R(p)$) and the transition probability (or Einstein Coefficient A_{pk}). Assuming the equations of CR model, the emissivity depends basically on n_e, T_e and n_0 according to the following formula:

$$\epsilon_{pk} = n_0 n_e X_{pk}^{eff}(T_e, n_e, \dots)$$

Using the ratio of emissivities $\epsilon_{H_\beta}/\epsilon_{H_\gamma}$, the direct dependence on particle density n_0 and n_e cancels out. The measured line ratio is then given by the ratio of the corresponding effective emission rate coefficient, which exhibit a dependence on n_e and $T_e[\,]$. The following formula for the ratio of emissivities is assumed, if electron collision excitation from H is the dominant channel:

$$\frac{\epsilon_{H_\beta}}{\epsilon_{H_\gamma}} = \frac{X_{H_\beta}^{eff,H}(T_e, n_e)}{X_{H_\gamma}^{eff,H}(T_e, n_e)} = \frac{R_{H_\beta}(p) \cdot A_{H_\beta}}{R_{H_\gamma}(p) \cdot A_{H_\gamma}}$$

Figure 4.6 shows the dependence of the ratio $\epsilon_{H_\beta}/\epsilon_{H_\gamma}$ on n_e for different values of T_e obtained from the CR model. The result of the CR model were interpolated with a cubic spline in order to obtain a trend of the emissivity ratios with n_e and T_e. Thus, comparing the experimental ratio of emissivities with the prediction of CR model it is possible to obtain an estimation of n_e. The ratio dependence on T_e is weak, so an initial T_e of 2 eV has been utilized. We will see in Section 4.4 that, given an electron density, an estimation of T_e from the data analysis is also possible. So using a recursive algorithm both T_e and n_e could be estimated.

4.2.2 Results

Figure 4.7 and Figure 4.8 show some results of n_e in function of RF power. The electron densities are in the order of $10^{17}\ \mathrm{m^{-3}}$ and it seems to slightly

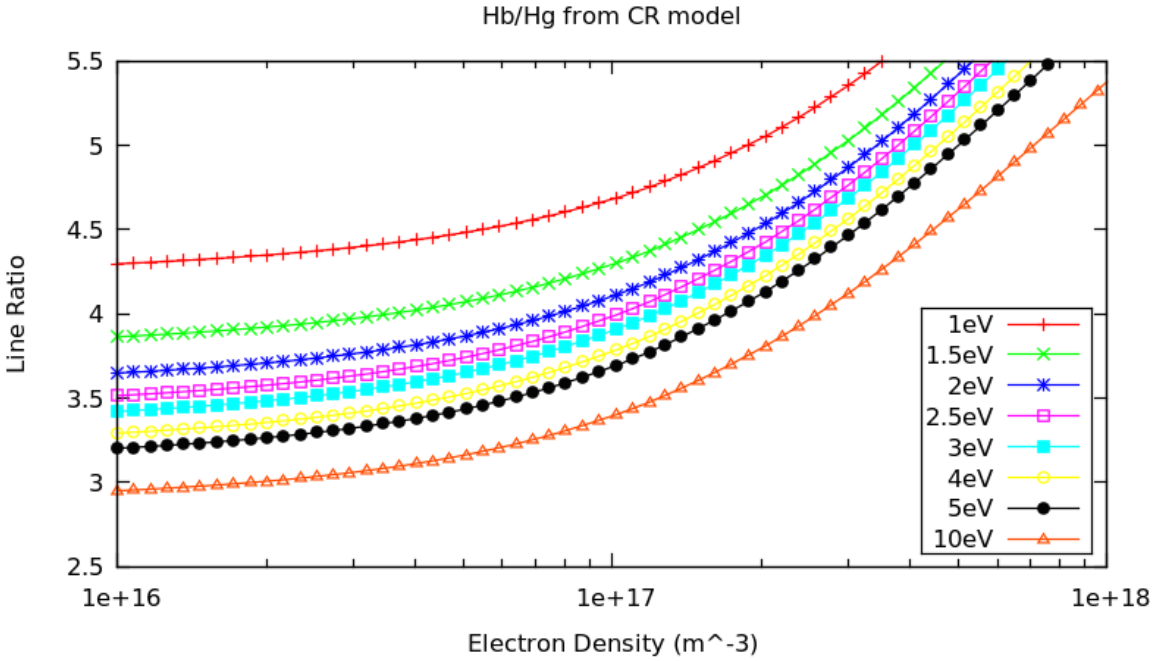

Figure 4.6: $\epsilon_{H_\beta}/\epsilon_{H_\gamma}$ ratio from CR Model as a function of n_e for different T_e

increase with the RF power injected. These results are comparable with what found in similar ion sources [32]. An error has been associated to n_e based on the gaussian fit errors. It consists of the difference between the maximum ($n_{e,max}$) and the minimum ($n_{e,min}$) value of electron density calculated by the following ratio of emissivities:

$$R_{max} = \frac{\epsilon_{H_\beta}}{\epsilon_{H_\gamma}} + \sigma_{\epsilon_{H_\beta}/\epsilon_{H_\gamma}}; R_{min} = \frac{\epsilon_{H_\beta}}{\epsilon_{H_\gamma}} - \sigma_{\epsilon_{H_\beta}/\epsilon_{H_\gamma}}$$

where $\sigma_{\epsilon_{H_\beta}/\epsilon_{H_\gamma}}$ is given by propagation using the errors of emissivities from the gaussian fit. Figure 4.7 and Figure 4.8 show the error-bars of n_e with the methods aforementioned. The other method applied, in order to rapidly give an estimate of the errors, is based on a variation of 10% of the emissivities. It starts from the following ratios:

$$R_{max} = \frac{\epsilon_{H_\beta} + 0.1 \cdot \epsilon_{H_\beta}}{\epsilon_{H_\gamma} - 0.1 \cdot \epsilon_{H_\gamma}}; R_{min} = \frac{\epsilon_{H_\beta} - 0.1 \cdot \epsilon_{H_\beta}}{\epsilon_{H_\gamma} + 0.1 \cdot \epsilon_{H_\gamma}}$$

and derives the corresponding $n_{e,max}$ and $n_{e,min}$. The two methods give comparable results for the estimation of experimental errors.

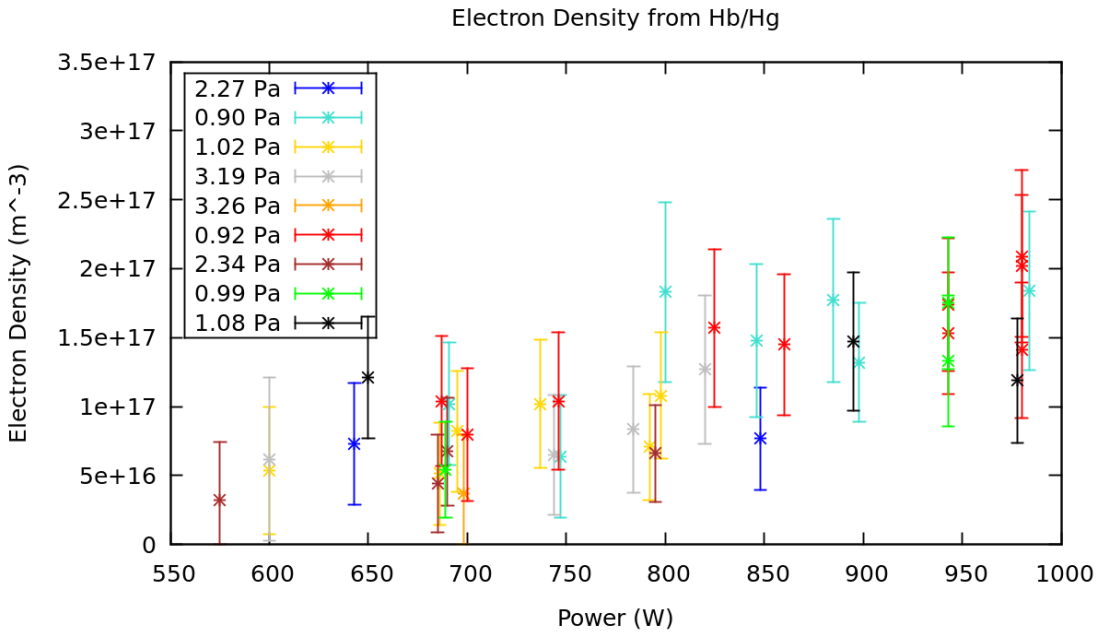

Figure 4.7: Electron Temperature as a function of power, low resolution spectrometer, filling pressure in the range [0.90:2.34] Pa

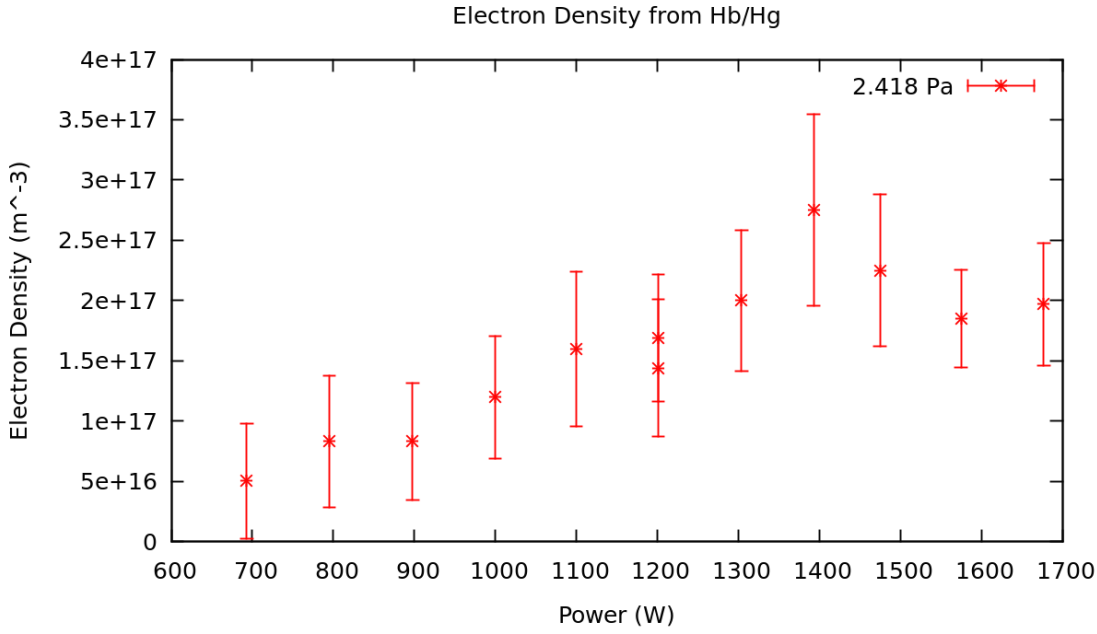

Figure 4.8: Electron Temperature as a function of power, low resolution spectrometer, filling pressure of 2.4 Pa

4.3 Dissociation Degree

4.3.1 Analysis Method

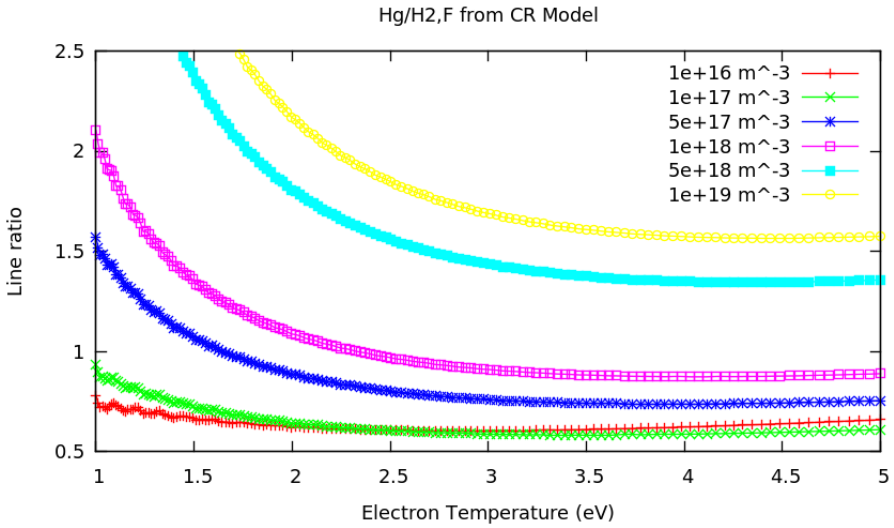

Figure 4.9: $\epsilon_{H_\gamma}/\epsilon_{H_{2,Fulch}}$ ratio from CR Model as a function of T_e for different n_e

The ratio of emissivities $\epsilon_{H_\gamma}/\epsilon_{H_{2,Fulch}}$ is well suited for the determination of the dissociation degree (n_H/n_{H_2}). According to the CR model, the emissivity of H_γ is given by:

$$\epsilon_{H_\gamma} = \epsilon_{52} = n_H(5)A_{52} = n_H n_e X^{eff,H}_{H_\gamma}(T_e, n_e)$$

In the same way, for $H_{2,Fulch}$ band:

$$\epsilon_{H_{2,Fulch}} = n_{H_2} n_e X^{eff}_{H_{2,Fulch}}(T_e, n_e)$$

Thus, the H_γ transition depends on the atomic hydrogen density (n_H), while the Fulcher band on the molecular hydrogen density (n_{H_2}). Figure 4.9 shows that the ratio of emission rate coefficients $X^{eff,H}_{H_\gamma}/X^{eff}_{H_{2,Fulch}}$ is almost independent from T_e and is only slightly dependent on n_e in the range $1 \cdot 10^{16}\mathrm{m}^{-3} < n_e < 1 \cdot 10^{18}\mathrm{m}^{-3}$. The following formula has been used to calculate the dissociation degree:

$$\frac{n_H}{n_{H_2}} = \frac{\epsilon_{H_\gamma}}{\epsilon_{H_{2,Fulch}}} \cdot \frac{X^{eff,H}_{H_{2,Fulch}}(n_e, T_e)}{X^{eff}_{H_\gamma}(n_e, T_e)}$$

where the emissivities come from the experimental data, while the ratio of the effective emission rate coefficients come from the CR model by fixing n_e and T_e to the values estimated[4]. The estimation of the Fulcher band emission has been multiplied by a factor of 2 because there are other contributions of radiation spontaneously emitted by H_2 that are not contained in the range 590÷640 nm considered for the Fulcher transition.

4.3.2 Results

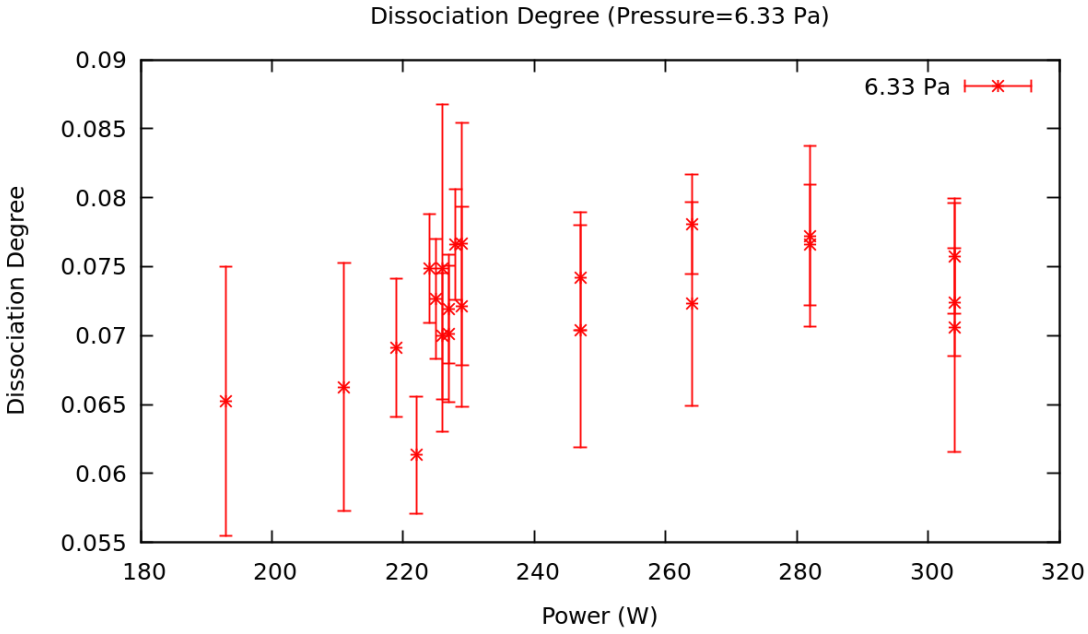

Figure 4.10: Dissociation Degree (n_H/n_{H_2}) as a function of power, filling pressure of 6.33 Pa

The dissociation degrees as a function of RF power and filling pressure of the source of NIO1 are shown in Figure 4.10 and Figure 4.11. From Figure 4.10, the dissociation degree seems to be constant with RF power applied in the range [180:320] W for filling pressure of 6.3 Pa. These results are in accord with the ones obtained in [32]. Figure 4.11 shows that for higher values of power, the dissociation degree decreases with the applied RF power. This result is due to the stronger increase of molecular radiation with respect to the atomic one (see Figure 4.5). This result is surprising,

[4]The T_e was assumed equal to 2 eV at start, and updated in the following iterations

since an increase of electron density and temperature should also increase the gas dissociation. A possible cause of this result is the presence of a reaction which enhances the molecular emissions or takes radiation from the Balmer emissions. Further investigations are in progress. The dissociation

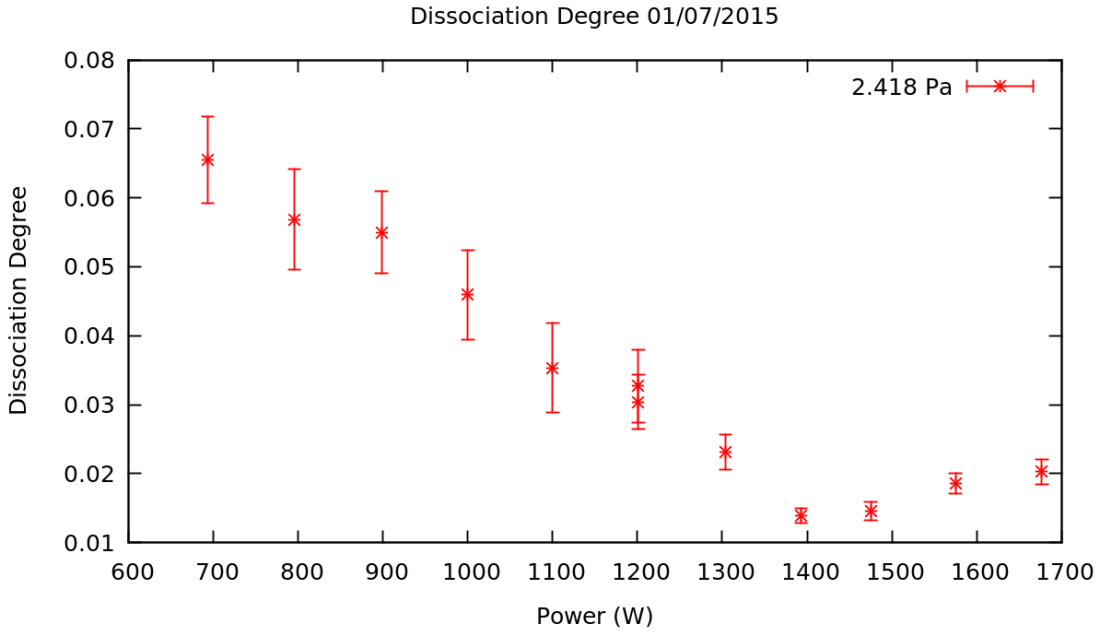

Figure 4.11: Dissociation Degree (n_H/n_{H_2}) in the NIO1 source as a function of power with gas pressure of 2.418 Pa

degree errors have been estimated as the difference between the maximum and minimum value of dissociation degree ($(n_H/n_{H_2})_{max}$ and $(n_H/n_{H_2})_{min}$ respectively) calculated with the following method:

- The maximum and minimum ratio of effective emission rate coefficient was derived from the CR model[5], fixing the electron density at $n_{e,max}$ and $n_{e,min}$: $\left(\frac{X^{eff,H}_{H_\gamma}}{X^{eff}_{H_{2,Fulch}}}(T_e, n_{e,max})\right)_{max}$ and $\left(\frac{X^{eff,H}_{H_\gamma}}{X^{eff}_{H_{2,Fulch}}}(T_e, n_{e,min})\right)_{min}$

- The maximum and minimum ratio of experimental emissivities was calculated according to the following formulas: $R_{max} = \frac{\epsilon_{H_\gamma}}{\epsilon_{H_{2,Fulch}}} + \sigma_{\epsilon_{H_\gamma}/\epsilon_{H_{2,Fulch}}}$ and $R_{min} = \frac{\epsilon_{H_\beta}}{\epsilon_{H_\gamma}} - \sigma_{\epsilon_{H_\beta}/\epsilon_{H_\gamma}}$ where $\sigma_{\epsilon_{H_\beta}/\epsilon_{H_\gamma}}$ comes from the gaussian fit described in Section 4.1.2.

[5]The CR model considered gives *the ratio* of the effective emission rate coefficients

- The maximum and minimum values of n_H/n_{H_2} were calculated with the following formulas: $(n_H/n_{H_2})_{max} = R_{max}/\left(\frac{X^{eff,H}_{H_\gamma}}{X^{eff}_{H_{2,Fulch}}}(T_e, n_{e,min})\right)_{min}$ and $(n_H/n_{H_2})_{min} = R_{min}/\left(\frac{X^{eff,H}_{H_\gamma}}{X^{eff}_{H_{2,Fulch}}}(T_e, n_{e,max})\right)_{max}$

Finally, the difference between $(n_H/n_{H_2})_{max}$ and $(n_H/n_{H_2})_{min}$ has been calculated. Like the estimation of n_e previously described, the procedure to deduce the dissociation degree is based on a recursive algorithm on T_e whose value was updated in the following iterations.

4.3.3 Atomic and Molecular Hydrogen Density

The *molecular hydrogen density* n_{H_2} has been deduced from the Dalton's law:

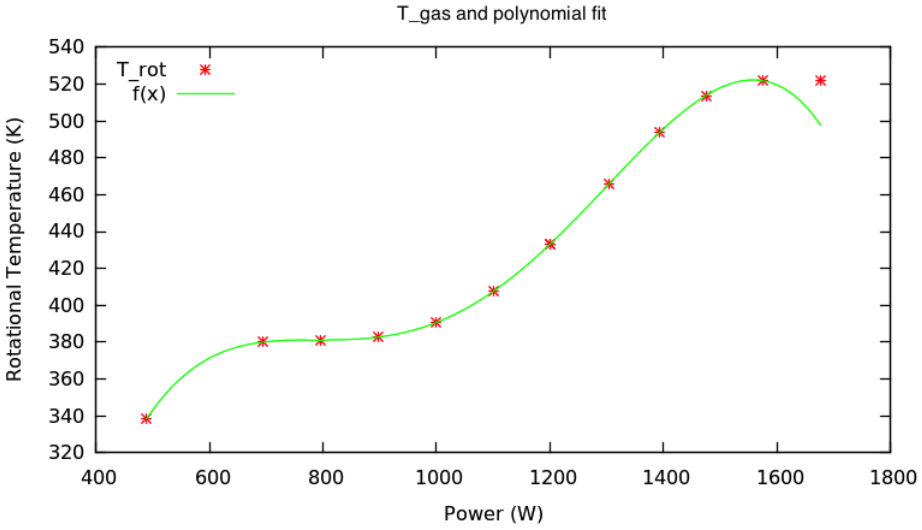

Figure 4.12: Gas Temperature T_g obtained as a function of RF power with the fitting 4^{th} degree polynomial

$$p_{source} = n_{H_2} k_B T_g$$

where k_B is the Boltzmann's constant, T_g is the gas temperature, and p_{source} the pressure of the gas filling the source. The pressures in the source are obtained by a calibration with the pressures measured in the vessel by a Pirani vacuum gauge, while the T_g is assumed equal to the rotational temperature. This temperature has been obtained from the Fulcher transition

analyzed with a high resolution spectrometer and using the slope of a Boltzmann graph [33]. The dependence of T_g on the RF power has been obtained by interpolating its values with a 4^{th} degree polynomial of the form:

$$y = -1.201 \cdot 10^{-9} \cdot x^4 + 5.019 \cdot 10^3 \cdot x^3 - 7.391 \cdot 10^{-3} \cdot x^2 + 46.50 \cdot x - 6.863 \cdot 10^2$$

where y is the $T_g[K]$ and x is the RF power applied (in W). Figure 4.12 shows the values of T_g obtained and the fitting polynomial.

The *atomic hydrogen density* n_H has been deduced by multiplying the dissociation degree (n_H/n_{H_2}) previously estimated with the molecular hydrogen density (n_{H_2}).

4.4 Electron Temperature

4.4.1 Analysis Method

The knowledge of n_e, n_H/n_{H_2} and n_H allow to estimate the electron temperature (T_e). Considering that the effective emission rate coefficient of H_γ is:

$$X^{eff,H}_{H_\gamma}(n_e, T_e) = \frac{\epsilon_{H_\gamma}}{n_e n_H}$$

where the terms on the right are known, being ϵ_{H_γ} the experimental emissivity of H_γ, while n_e and n_H come from the estimates previously found. A comparison between the estimated $X^{eff,H}_{H_\gamma}(n_e, T_e)$ and the results of the CR model gives T_e.

The values of $X_{H_\gamma}(n_e, T_e)$ predicted from the CR model are shown in Figure 4.13 as a function of T_e .

4.4.2 Results

The results of the estimates of T_e are shown in Figure 4.14.

From these results the electron temperature seems to be in the order of some eV and it increases slightly with the applied RF power, while in the correspondence of the E-H mode transition it seems to present a steep growth with the applied RF power.
The experimental errors were estimated with the following method:

- The values of effective emission rate coefficients $X^{eff,H}_{\epsilon_{H_\gamma}}(T_e, n_{e,max})$ and $X^{eff,H}_{\epsilon_{H_\gamma}}(T_e, n_{e,min})$ corresponding to the values of $n_{e,max}$ and $n_{e,min}$ respectively were calculated from the CR model

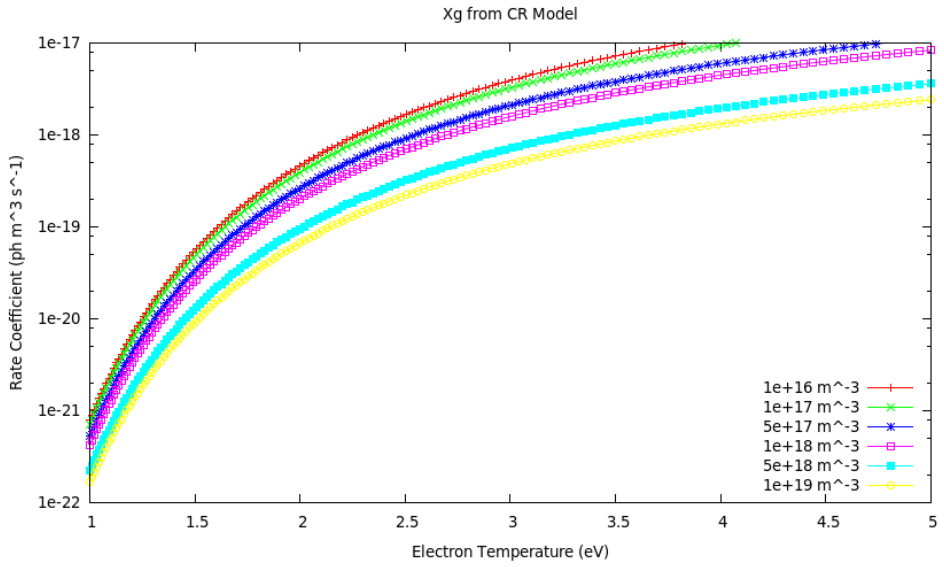

Figure 4.13: Effective emission rate coefficient ($X^{eff,H}_{H_\gamma}$) of the H_γ transition from the CR Model

- The maximum and minimum value of effective emission rate coefficients has been calculated from the experimental emissivities obtained, according to the following formulas:

$$X^{eff;H}_{\epsilon_{H_\gamma},min}(T_e, n_{e,max}) = \frac{\epsilon_{H_\gamma} - \sigma_{\epsilon_{H_\gamma}}}{n_H \cdot n_{e,max}};$$

$$X^{eff;H}_{\epsilon_{H_\gamma},max}(T_e, n_{e,min}) = \frac{\epsilon_{H_\gamma} + \sigma_{\epsilon_{H_\gamma}}}{n_H \cdot n_{e,min}}$$

The following electron temperatures were estimated with a combination of the parameters previously described:

Electron Temperature	Rate Coeff Estimated	Rate Coeff of CR model
$T_{e,21}$	$X^{eff;H}_{\epsilon_{H_\gamma},min}(T_e, n_{e,max})$	$X^{eff,H}_{\epsilon_{H_\gamma}}(T_e, n_{e,max})$
$T_{e,22}$	$X^{eff;H}_{\epsilon_{H_\gamma},max}(T_e, n_{e,min})$	$X^{eff,H}_{\epsilon_{H_\gamma}}(T_e, n_{e,max})$
$T_{e,31}$	$X^{eff;H}_{\epsilon_{H_\gamma},min}(T_e, n_{e,max})$	$X^{eff,H}_{\epsilon_{H_\gamma}}(T_e, n_{e,min})$
$T_{e,32}$	$X^{eff;H}_{\epsilon_{H_\gamma},max}(T_e, n_{e,min})$	$X^{eff,H}_{\epsilon_{H_\gamma}}(T_e, n_{e,min})$

The difference between the maximum and the minimum value of the previously estimated electron temperatures has been assumed as an experimental error of T_e.

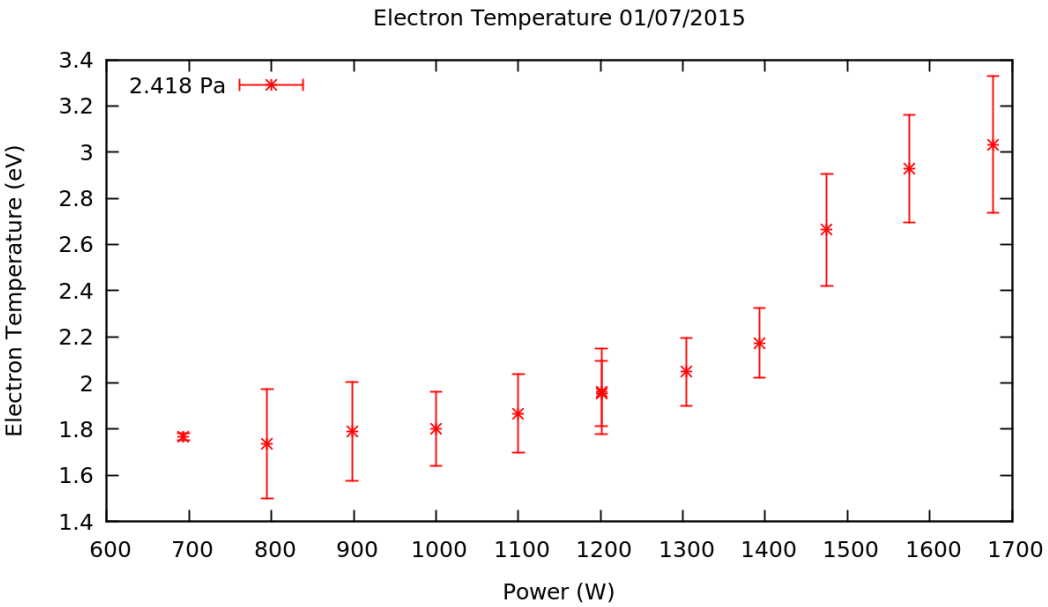

Figure 4.14: Electron Temperature T_e in the NIO1 source with gas pressure of 2.418 Pa

Chapter 5

Conclusions

Neutral beam heating systems have been very successful in heating many present day tokamaks to reactor temperatures needed for fusion processes. These beam systems have been driven by positive ions accelerated up to 100 keV. However, typical reactor dimensions and densities are higher than in present day experiments. In order to fulfill these conditions, high beam energies are required, on the order of 1 MeV. Since positive ion efficiency decreases rapidly above 100 keV, a program to develope and investigate high-energy negative ion beam injectors that maintain high efficiency at 1 MeV level has been created. In this scenario, the NIO1 experiment has been developed in collaboration between Consorzio RFX and INFN-LNL with the aim of optimizing both the production of negative ions and their extraction and beam optics. Its small dimensions and manageability allow several diagnostics on the source and the extracted beam. In particular, this thesis investigated plasma parameters of the NIO1 source by means of an Optical Emission Spectroscopy. This technique is well suited to determine averaged plasma parameters in different experimental conditions (i.e. with different RF power and gas pressure of the source). In this thesis both the results obtained with air and hydrogen as a filling gas were presented. Analyzing the emission spectra with air as a filling gas, the following conclusions could be deduced:
The electron temperature seems to decrease with the applied RF power for low gas pressures, while it does not depend on the RF power for higher values of pressure. The difference between the estimates deduced from measurements with low and high resolution spectrometers and the previsions of the numerical models indicates that this analysis method have to be improved in order to obtain better results. These results of emission spectroscopy suggest that probably the corona model is quite unsophisticated and it has to be corrected with a more appropriate CR model that includes more reactions.

The vibrational temperatures increase with the increasing RF power, more rapidly until 100/125 W and then saturate. The rotational temperatures are in the order of 450 K.
The estimations of plasma parameters with hydrogen as a filling gas have been made possible through a comparison of the experimental emissivities with the prediction of a Collisional-Radiative model. The electron density and electron temperature deduced are respectively in the order of $10^{17}\mathrm{m}^{-3}$ and some eV and increase with the RF power. These results are comparable with the ones obtained in other experiments. The dissociation degree (n_H/n_{H_2}) is in the order of some percent. At fixed gas pressure of 2.4 Pa, n_H/n_{H_2} seems to decrease with the applied RF power for values of power in the range $500 \div 1700$ W. The decrease of the dissociation degree deserves further investigations because the H_γ and Fulcher emissions are enhanced by the electron density and temperature. Probably other reactions have to be taken into account in the model utilized, these reactions seem to take radiation from the Balmer emission. At fixed gas pressure of 2.4 Pa, increasing the RF input power in the range $1400 \div 1700$ W, a E-H mode transition (capacitive to inductive coupling) is registered. This transition is accompanied by a sudden jump in the light emission, in particular in the Fulcher band. In future experimental campaigns it will be possible to collect more data for pressure down to 0.3 Pa and values of RF power up to 2500 W with particular attention to the E-H transition. Since the line ratio method is sensitive to the estimations of the emissivities, the measurements with high resolution spectrometers could help to distinguish the background lines from the transitions considered in order to reduce the errors of the estimated emissivities. The development of a more sophisticated interpretative model could also help to investigate the trends and values of plasma parameters with RF power and gas pressure by means of OES. Finally, the extracted beam will be investigated by means of beam emission spectroscopy in order to obtain the divergence and the beam profile.

Bibliography

[1] R.A. Hinrichs, M. Kleinbach, *Energy: Its Use and the Environment*, Brooks/Cole, Fifth Edition, 2013

[2] J. Freidberg, *Plasma Physics and Fusion Energy*, Cambridge University Press, 2007

[3] F.F. Chen, *Introduction to Plasma Physics and Controlled Fusion*, Plenum Press, Second Edition, 1974

[4] ITER official website, `http://www.iter.org`

[5] `http://www-diva.eng.cam.ac.uk/mphil-in-nuclear-energy/external-lectures/2012-13-seminars/fusion-power-and-the-engineering-challenge`

[6] R.V. Budny, *Comparisons of predicted plasma performance in ITER H-mode plasmas with various mixes of external heating*, Nucl. Fusion 49, 085008, 2009

[7] *Agreement on the Establishment of the ITER International Fusion Energy Organization for the Joint Implementation of the ITER Project*, INFCIRC/702, 25 April 2007

[8] I.G. Brown, *The Physics and Technology of Ion Sources*, Wiley-VCH Verlag GmbH & Co. KGaA, 2003

[9] R.S. Hemsworth, T. Inoue, *Positive and Negative Ion Sources for Magnetic Fusion*, IEEE Trans. Plasma Sci., 33, 6, 2005

[10] M. Cavenago, *INFN contribution to Neutral Beam Injectors at RFX and NIO1*, Oral presentation at Miniworkshop on Accelerators, Legnaro, 17 February 2015

[11] M. Cavenago et al., *Ion beams for ITER*, Oral presentation at WP4 (AccApplic) Parallel Session, 1st EUCARD2 Annual Meeting, Hamburg, Germany, 21 May 2014

[12] M. Cavenago, V. Antoni, G. Serianni, P. Veltri, T. Kulevoy, S. Petrenko, *NIO1 a versatile negative ion source*, Proceedings of IPAC'10, Kyoto, Japan, 2010

[13] M. Cavenago et al., *Development of Versatile Multiaperture Negative Ion Sources*, Rev Sci Instrum. (2012)

[14] B. Zaniol et al, *NIO1 Diagnostics*, AIP Conf. Proc. 1655, 060010 (2015)

[15] A. Mimo, *Diagnostics for negative ion source NIO1*, Master Thesis, Università degli Studi di Padova, Physics and Astronomy Department, 2014

[16] M. Cazzador, *Analytical and numerical models and first operations on the negative ion source NIO1*, Master Thesis, Università degli Studi di Padova, Physics and Astronomy Department, 2014

[17] W. Ubachs, *Notes on: Molecular Physics*, Vrije Universiteit, Amsterdam, 2004

[18] L.E. Gumley, *Practical IDL Programming*, Morgan Kaufmann Publishers, First Edition, 2001

[19] `www.hamamatsu.com/eu/en/4016.html`

[20] C. Braggio, *Laboratorio di Fisica (MOD A): Corso di Laurea in Fisica SC1158*, A.A. 2013/2014

[21] `http://www.phy.ohiou.edu/~mboett/astro401_fall12/broadening.pdf`

[22] `http://astrowww.phys.uvic.ca/~tatum/stellatm/atm10.pdf`

[23] N. Britun et al., *Determination of the vibrational, rotational and electron temperatures in N_2 and Ar-N_2 rf discharge*, J. Phys. D: Appl. Phys. 40 1022-1029 (2007), `DOI:10.1088/0022-3727/40/4/016`

[24] N. Chandwani, M.B.Chowdhuri, S.K.Nema, S.Mukherjee, *Determination of Rotational, Vibrational and Electron Temperatures in Dielectric Barrier Discharge in air at atmospheric pressure*, Technical Report (2014), `DOI:10.13140/RG.2.1.2078.6725`

[25] H.-J. Kunze, *Introduction to Plasma Spectroscopy*, Springer-Verlag, 2009

[26] U. Fantz, *Atomic and Molecular Emission Spectroscopy in Low Temperature Plasmas Containing Hydrogen and Deuterium*, IPP-Report, 10/21, March 2002

[27] T. Fujimoto, *Plasma Spectroscopy*, Clarendon Press-Oxford, 2004

[28] U. Fantz, *Basics of plasma spectroscopy*, Plasma Sources Sci. Technol. 15, S137-S147 (2006), DOI:10.1088/0963-0252/15/4/S01

[29] D. Wünderlich, S. Dietrich, U. Fantz, *Application of a collisional radiative model to atomic hydrogen for diagnostic purposes*, Journal of Quantitative Spectroscopy & Radiative Transfer 110, 62-71, 2009

[30] U. Fantz, D. Wünderlich, *Atomic and Molecular Collisional Radiative Modeling for Spectroscopy of Low Temperature and Magnetic Fusion Plasmas*, AIP Conference Proceedings 1344, 204, 2011, DOI:10.1063/1.3585820

[31] U. Fantz, D. Wünderlich, *A novel diagnostic technique for H^- (D^-) densities in negative hydrogen ion sources*, New Journal of Physics 8, 301 (2006), DOI:10.1088/1367-2630/8/12/301

[32] U. Fantz et al., *Spectroscopy-a powerful diagnostic tool in source development*, Nucl. Fusion 46, S297-S306, 2006, DOI:10.1088/0029-5515/46/6/S10

[33] M. Barbisan et al., *First hydrogen operation of NIO1: characterization of the source plasma by means of an optical emission spectroscopy diagnostic*, 16th International Conference on Ion Source, New York, USA, August, 2015

Ringraziamenti

Ringrazio innanzitutto il Dott.Gianluigi Serianni che mi ha permesso di svolgere questo lavoro di tesi e mi ha trasmesso almeno un po' della sua passione riguardo le attività svolte dal Consorzio Rfx e la Dott.ssa Barbara Zaniol che mi ha iniziato alla spettroscopia con pazienza e con il sorriso, sempre disponibile per consigli o spunti di lavoro. Tra le altre persone che hanno permesso il mio lavoro di tesi, ringrazio la Dott.ssa Lorella Carraro e il gruppo di dottorandi/post-doc, in particolare il Dott.Marco Barbisan e Dott.Carlo Baltador che, oltre a fornirmi ad ottimi spunti, mi hanno aiutato ad ambientarmi.
Tante, poi, sono le persone che ho conosciuto in questi tre anni di Università che mi hanno arricchito a livello personale. Tra queste una particolare menzione va al gruppo di studenti/sse della Facoltà di Fisica che hanno contribuito a formare un gruppo coeso di amici, prima che colleghi o compagni di banco.
Ultimo, ma non in ordine di importanza, è il ringraziamento alla mia famiglia che mi ha sempre sostenuto e creduto in me.
Con la speranza che i prossimi due anni universitari siano altrettanto utili per una mia crescita sia come fisico che come persona.